INFORMATION TO USERS

This manuscript has been reproduced from the microfilm master. UMI films the text directly from the original or copy submitted. Thus, some thesis and dissertation copies are in typewriter face, while others may be from any type of computer printer.

The quality of this reproduction is dependent upon the quality of the copy submitted. Broken or indistinct print, colored or poor quality illustrations and photographs, print bleedthrough, substandard margins, and improper alignment can adversely affect reproduction.

In the unlikely event that the author did not send UMI a complete manuscript and there are missing pages, these will be noted. Also, if unauthorized copyright material had to be removed, a note will indicate the deletion.

Oversize materials (e.g., maps, drawings, charts) are reproduced by sectioning the original, beginning at the upper left-hand corner and continuing from left to right in equal sections with small overlaps. Each original is also photographed in one exposure and is included in reduced form at the back of the book.

Photographs included in the original manuscript have been reproduced xerographically in this copy. Higher quality 6" x 9" black and white photographic prints are available for any photographs or illustrations appearing in this copy for an additional charge. Contact UMI directly to order.

U·M·I

University Microfilms International
A Bell & Howell Information Company
300 North Zeeb Road, Ann Arbor, MI 48106-1346 USA
313/761-4700 800/521-0600

Order Number 9132432

Interference between different optical processes

Chen, Ce, Ph.D.

Purdue University, 1991

U·M·I
300 N. Zeeb Rd.
Ann Arbor, MI 48106

Graduate School Form 9
(Revised 8/89)

PURDUE UNIVERSITY
GRADUATE SCHOOL
Thesis Acceptance

This is to certify that the thesis prepared

By Ce Chen

Entitled

Interference between Different Optical Processes

Complies with University regulations and meets the standards of the Graduate School for originality and quality

For the degree of Doctor of Philosophy

Signed by the final examining committee:

Daniel S Elliott, chair

E L O

E R Grant

S Datta

Approved by:

Richard Schwartz
Department Head

4/4/91
Date

This thesis ☐ is ☒ is not to be regarded as confidential

Daniel S Elliott
Major Professor

INTERFERENCE BETWEEN DIFFERENT OPTICAL PROCESSES

A Thesis

Submitted to the Faculty

of

Purdue University

by

Ce Chen

In Partial Fulfillment of the

Requirements for the Degree

of

Doctor of Philosophy

May 1991

This thesis is dedicated

to the memory of

my Father and Mother

ACKNOWLEDGEMENTS

I would like to express my deep thanks to my Major Professor Daniel S. Elliott for his giving me the opportunity to carry out this project, for his valuable academic advices, technical guidance and joint laboratory work.

I would also like to thank the other members of my PhD Advisory Committee - Drs. Chin-Lin Chen, Edward Grant and Supriyo Datta for their valuable time and interest in my work.

Each of the students who have worked in our laboratory group has provided friendship and contribution. Yiyian Yin, in particular, has provided numerous conversations and helps throughout this project. Help and encouragement from Nader Pakdaman, Ralf Nentwig, Cheng Xie, Gerhard Klimeck and Ed Bodette are also appreciated.

I would also like to thank those who provided the resources necessary for completing this project. Mr. Claude Harrington in Machine Shop, Mr. David Azpel and others in Instrument Room are appreciated for their great help.

I would like to thank wholeheartedly my wife Yi Wu, my daughter Xijia Chen, my parents-in-law and my sisters for their understanding, encouragement and support. Without their cooperation, I would not have been able to

complete my graduate study.

This work is supported by National Science Foundation, Grant No. ECS-8451259. Support from Purdue University through David Ross grant is also appreciated.

TABLE OF CONTENTS

Page

LIST OF TABLES

LIST OF FIGURES

Figure Page

ABSTRACT

Chen, Ce. Ph.D., Purdue University, May 1991. Interference between Different Optical Processes. Major Professor: Dr. Daniel S. Elliott.

This thesis reports an experimental study of an interference phenomenon between one-photon and three-photon $6s^1S_0$ - $6p^1P_1$ transition amplitudes in a vapor of atomic mercury. The interference was observed by monitoring the multiphoton ionization signal. Using a three-cell design we were able to separate the third-harmonic generation process and the interfering absorption processes such that we could externally control the relative phase between the two transition amplitudes and directly study the interference phenomena.

We observed that the multiphoton ionization signal, which is a measure of the net transition moment, varied sinusoidally as the relative phase increased. Using an eight-electrode design to collect the electrons ionized at different positions along the beam axis around the focal region, we measured the phase shift of the interference due to the π phase shift of a focused Gaussian beam propagating through the focal region. The experimental setup and the experimental procedure are discussed in detail. This new method can be used in the study of many phase sensitive processes including potential applications in coherent control of chemical reactions.

CHAPTER 1
INTRODUCTION

1.1 Introduction to the Interference Experiment

The work reported here is an experimental investigation of an interference phenomenon between the transition moments associated with a linear atomic interaction with a laser field and a nonlinear interaction with another laser field. This interaction of an atom with a multi-frequency field is qualitatively much different from interactions which have been studied in the past.

A common feature of previously studied processes is that each frequency component of the radiation field induces a different atomic or molecular transition, and the interaction of the atom or molecule with each component of the field can be followed in a stepwise fashion. A few examples of these effects are found in resonantly-enhanced multiphoton absorption, optical pumping, and state selective photodissociation.

More recently, a new type of interaction between an atomic system and a multi-frequency field has been reported [1, 2, 3, 4]. In these interactions, different processes are involved in the transition between two states. A few examples of this are the interaction involving multiphoton ionization and third-harmonic generation[5, 6, 7, 8, 9, 10], the interaction involving amplified spontaneous emission and four-wave mixing[11], the interaction involving

two-photon absorption and two-photon resonant sum frequency generation[12] and the interaction involving multiphoton ionization and stimulated Raman scattering[13]. As an example, consider the generation of third-harmonic radiation using an atomic vapor which has a transition nearly resonant with three times the frequency of the laser radiation. Two frequencies of radiation are present, these being the frequency incident upon the vapor and the frequency generated in the vapor. Both of the components of the radiation field can be considered to be nearly resonant with the atomic transition of the vapor; one by a direct single-photon transition, and the other by a nonlinear interaction involving the simultaneous absorption of three photons of the lower frequency field. In this case, the atom is effectively a two-level system, and each of the two components of the radiation are individually capable of exciting the atom from the ground state to the upper state. The presence of two "pathways" by which the transition can occur suggests the possibility of an interference process.

This interference has been suggested as one possible explanation for recent observations of a competition between the processes of resonantly-enhanced multiphoton ionization and third-harmonic generation in atomic vapors [1, 2, 3, 4]. Under certain conditions atomic vapors demonstrate a lower multiphoton ionization rate at high vapor densities than at low vapor densities. This was quite an unexpected result since the ionization current should be proportional to the number of atoms in the interaction region. Third-harmonic radiation was generated simultaneously in the vapor, and the correlation between the increased third-harmonic generation and the decreased multiphoton ionization has been verified by the reappearance of the ionization

current under conditions for which third-harmonic generation is precluded. For example, third-harmonic radiation can not be generated by standing wave excitation, or by circularly polarized radiation, because of wave vector phase matching and angular momentum conservation requirements. Three-photon resonantly-enhanced multiphoton ionization through the $6s$ and $6s'$ levels in xenon, disappearing at pressures above a few Torr under linearly polarized laser excitation, gives rise to sharp intense ionization signals under counterpropagating circularly polarized laser excitation[14] or counterpropagating linearly polarized laser excitation[1]. The large increase of the multiphoton ionization signal that occurs in the absence of third-harmonic generation is a direct experimental evidence that they are competing processes. The nonlinear interference process which is reported here has been suggested as a possible explanation of this competition, i.e. the net transition rate from the atomic ground state to the resonant intermediate state is decreased because of the destructive interference between the two transition pathways at the presence of the third-harmonic generation induced by the incident laser field, and hence the multiphoton ionization rate is decreased.

A very important distinction should be drawn between this interference process and other interference processes in atomic physics. Interference effects in spectroscopy which have been studied to date are similar in that the different pathways by which the interaction can proceed involve multiple intermediate states of the atoms. Quantum beats, for example, display the evolution of a coherently excited superposition of atomic wavefunctions through the time dependence of their radiative fluorescence[15] or photoelectron angular distributions[16, 17]. A periodic time dependence can

be detected in these signals with observed frequencies being related to energy differences among the nearly degenerated levels of the excited state. Another interference phenomenon can be found in multiphoton absorption processes, where competition among intermediate levels can result in a nearly complete cancellation of the transition probability[18, 19]. When the laser is tuned to a frequency greater than the transition frequency for one intermediate state, and lower than the other, the transition amplitudes for these two multiphoton pathways are of opposite sign and the sum will equal zero at the proper detuning.

The experiment reported here is a demonstration and investigation of an atomic interference phenomenon which depends upon the coherence of the electromagnetic radiation with which the atom is interacting. The interference in this case is due to the "choice" of the atom to interact with either of two components of the radiation field, one of which can be absorbed linearly, and the other by means of nonlinear process. The relative phase of the two components of the field is expected to be of critical importance in this experiment. The competition between a linear and a nonlinear interaction sets this process apart from interference processes which have been studied previously. The number of observations of competition between optical processes has been growing steadily in the past few years because of the increasing power available from laser sources and the advances which have been made in generation of coherent UV and VUV radiation by harmonic generation and sum or difference frequency generation techniques. In the experiments, so far, the competing processes are proceeding in the same region, and a separation of the two processes for closer examination would

produce significant insight into the interaction. This separation is, in essence, the key to the program reported here, and allows for the careful control of the relative phase of the two optical fields. The capability of the control of the relative phase makes the experiment a new method in the study of this new type of optical processes.

1.2 Significance of this Interference Experiment

Resonantly-enhanced harmonic generation and sum frequency techniques are being widely explored as sources of high resolution, coherent, ultraviolet radiation. The interference processes involved in this investigation are important for the complete understanding and applications of nonlinear interactions. The generation of higher harmonics which commonly accompanies the use of high power lasers makes the study of this process particularly relevant.

To actively control the direction of chemical reactions has been a longstanding goal for scientists. Early laser-based attempts at control relied either on the use of high power of lasers to alter the dynamics, or on the frequency or temporal resolution of the laser fields. Both methods suffer from severe drawbacks, the former requires too high laser power to be practically manageable in laboratory and the experiments based on frequency or temporal resolution have been generally disappointing [20]. Recently, an alternative approach named "coherent radiative control" has been proposed[21, 22, 23, 24, 25, 26]. The authors have shown by their computational results that the product distribution of some chemical reactions can be actively controlled over a vast range. As discussed in the next chapter,

to carry out their idea of controlling chemical reactions will depend on the experimental techniques very similar to those that we have developed in our interference experiments. The importance of our experiments lies not only in their significant results but also in the potential applications of the methods and techniques in other areas.

1.3 Structure of this Thesis

A general description of the interference experiment, its distinction from other works, and the significance have been reported in Chapter 1.

Chapter 2 is devoted to a survey of related works by other scientists and researchers, in which we will discuss a series of experimental results showing the "competition" between different optical processes; the theoretical explanations for this "competition" phenomena, especially the concept of "phase locking" and "optical balance"; and the new theoretical developments in controlling over chemical reactions, called "coherent radiative control".

In Chapter 3, we will derive a mathematical expression for the net ionization rate in the interference experiment using focused Gaussian beam. Based on that formula, we will discuss the requirements and conditions which will allow us to observe the interference between different optical processes. These discussions will be useful to many phase sensitive processes.

In Chapter 4, we will describe in detail the experimental setups for the interference experiments and the underlying physics of the design. This chapter can be considered as the materialization of the theoretical considerations discussed in the previous chapter. The similar design of this setup can be used in many phase sensitive experiments.

All the experimental results will be reported in Chapter 5, including results from single-cell experiment, three-cell experiment and eight-electrode three-cell experiment. Some details of the experimental setup related only to one specific experiment will be given in this chapter where that particular experiment is reported.

Chapter 6 will draw the conclusions for the experiments reported in this thesis.

CHAPTER 2
REVIEW OF PRIOR WORKS

As mentioned before, in the interactions of atoms with multi-frequency fields, different optical processes can be involved in a transition between two states. The existence of two distinct pathways make those interactions different from those studied in the past. Much effort has been made towards the understanding of this new type of interactions since the competition between the resonant multiphoton ionization and third-harmonic generation was investigated for the first time by J. C. Miller *et al* in 1980. These studies have very interesting and at times unexpected results.

2.1 Interactions Involving Resonantly-enhanced Multiphoton Ionization and Third-harmonic Generation

In studying five-photon multiphoton ionization of Xe at pressures ranging from 1 to 100 Torr, K. Aron and P. M. Johnson[27] focused attention on the unexpected and (previously) unexplained absence of a three-photon enhancement by the $5p^5 6s\,(^2P_{3/2}{}^o)$ J=1 state (labeled $6s$) at 68045.67 cm^{-1}. In contrast, working at lower Xe pressure (<1 Torr), J. C. Miller *et al.*[5, 6] observed resonantly-enhanced multiphoton ionization near the $6s$ state (see Figure 2.1). They noted the gradual weakening of the multiphoton ionization signal with increasing Xe pressure. The strong $6s$ ionization signal disappears

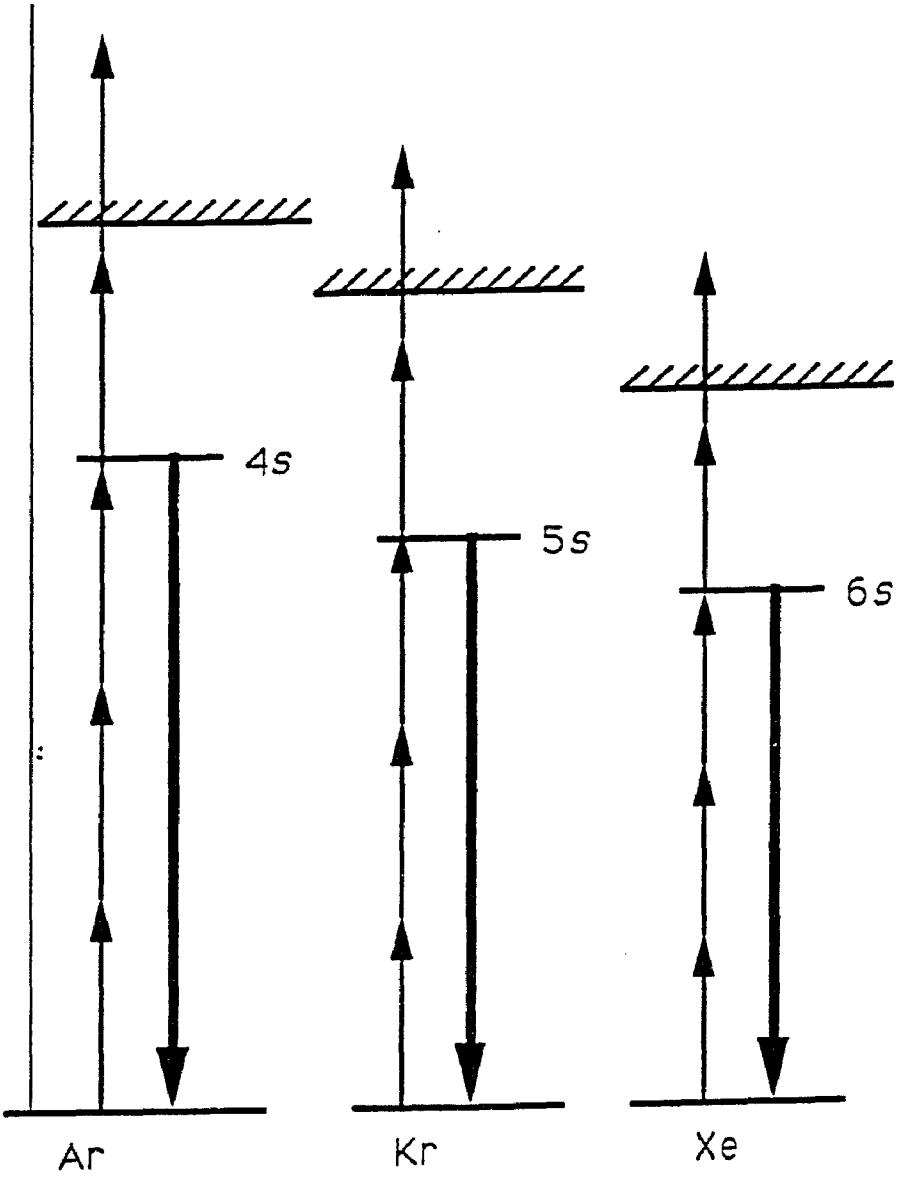

Figure 2.1. Energy-level diagram showing multi-photon ionization (MPI) and third harmonic generation (THG) in argon, krypton and xenon.

at a pressure greater than 0.30 Torr, accompanied by the production of intense third-harmonic radiation in the forward direction relative to pump laser. The third-harmonic emission is characterized by its laser excitation spectrum which exhibits larger shifts and wider linewidth comparing with the low-pressure observations. Similar results are found in krypton and argon. In krypton, the multiphoton ionization and third-harmonic generation spectra in the region of the $5s\,(3/2)^{\circ}, J$=1 resonance line follow the same pattern as seen for the $6s$ region of xenon. At low pressure ($\sim$ 0.3 Torr) both multiphoton ionization and third-harmonic generation are observed at the resonance position, with the same band shape. As the pressure increases, both peaks shift to blue and are broadened. The multiphoton ionization signal decreases in intensity and can not be observed above 2 Torr, while the third-harmonic generation continues to broaden and shift to blue. And for argon, the multiphoton ionization through $4s\,(3/2)^{\circ}, J$=1 level could not be observed above 5 torr. The third-harmonic generation in the argon experiment was not monitored due to the lack of a filter to separate it (106.7 nm) from the fundamental (320 nm). They initially interpreted their observations in terms of a complex theoretical model, based on collective emission, in which enhanced third-harmonic generation competes with multiphoton ionization. Subsequently, they developed a model based on the fact that the three-photon Rabi flopping frequency and the one-photon Rabi flopping frequency are equal and opposite in sign near resonance[28, 29].

J. H. Glownia and R. K. Sander[7] chose carbon monoxide in their study and observed competition between three- photon resonantly-enhanced third-harmonic generation and six-photon ionization by using the A state. To the

blue of R-head, ionization signals can no longer be detected, and only signals due to the third-harmonic radiation are observed in the forward direction with respect to the pump laser. The excitation spectrum exhibits increasing blue shifts and bandwidth with increasing pressure. By calculating the refractive index, they concluded that the blue shift and broadening of the third-harmonic generation with increasing pressure are consistent with the wave vector phase matching requirements. They proposed that the high ionization and dissociation limits for carbon monoxide suggest its use in generating coherent tunable vacuum ultraviolet radiation.

D. Normand, *et al.* [10] reported collective effects in resonantly-enhanced multiphoton ionization of mercury atoms whose spectrum provides an extended choice of resonant transitions accessible to tunable dye lasers compared with rare gas atoms. They investigated three resonantly enhanced multiphoton ionization processes (see Figure 2.2), (a) four-photon ionization through a three-photon resonance on the $7p\,^1P_1$ level, (b) five-photon ionization through a three-photon resonance on the $6p\,^1P_1$ level and (c) five-photon ionization through a four-photon resonance on the $6d\,^1D_2$ or $^3D_2$ levels. Ions or electrons from ionization were collected and the vacuum ultraviolet radiation generated in mercury vapor was measured simultaneously along the laser axis. When the pump dye laser wavelength is scanned around 420.8nm, the four-photon ionization signal, (the process listed as (a) above), exhibits a very sharp resonance of about the laser linewidth. Its maximum amplitude depends linearly on the mercury vapor pressure. No third-harmonic generation is reported. The linear dependence of the multiphoton ionization on the vapor pressure is just as expected since multiphoton

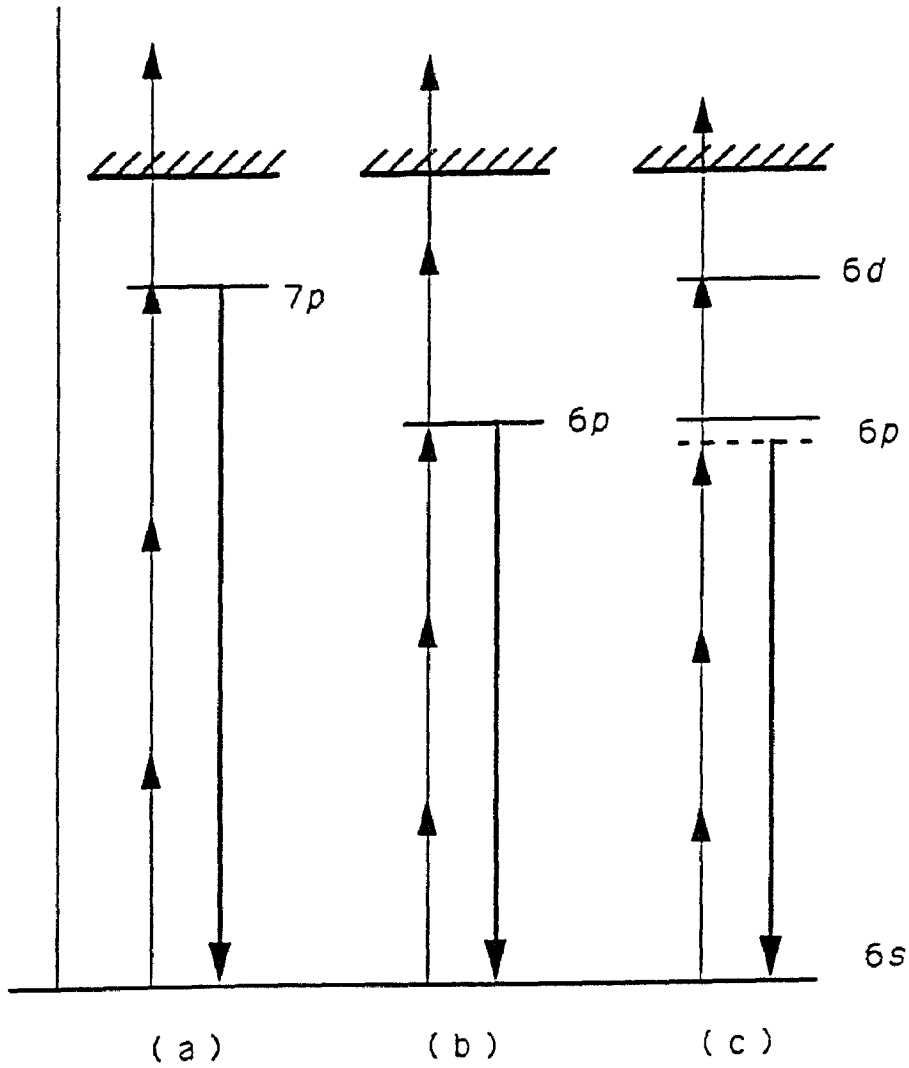

Figure 2.2. Energy-level diagram showing multi-photon ionization (MPI) and third harmonic generation (THG) in mercury.

ionization is the only channel of the interaction between the laser field and the atom. However, in the case of five-photon ionization, (processes listed as (b) and (c) above), the situation is completely different. Firstly the resonances appear much wider, accompanied by the generation of intense vacuum ultraviolet radiation, and secondly the pressure dependence of the multiphoton ionization signal is no longer linear but levels off for $6d$ resonances, or even decreases for the $6p$ resonances, with increasing ultraviolet generation. The different behaviors of multiphoton ionization in the presence and the absence of third-harmonic generation show again that these two processes are competing processes. This competition starts at relatively low pressure (below 10^{-3} Torr) and tends to favor third-harmonic generation at higher pressures whereas multiphoton ionization is dominant at low pressures. In particular, it was the first report about an observation of the third-harmonic generation enhanced by a four-photon resonance.

2.2 Interactions Involving Amplified Spontaneous Emission and Four-wave Mixing

M. S. Malcuit *et al*[11] reported the results of an experimental study that demonstrates competition between the amplified spontaneous emission and the four-wave mixing processes (see Figure 2.3). An intense laser beam was tuned around the $3s \longrightarrow 3d$ two-photon allowed transition of the sodium atom and the radiation emitted by the vapor cell was examined in both the forward and backward directions. They observed that a four-wave mixing process led to the generation of radiation near the $3d \longrightarrow 3p$ and $3p \longrightarrow 3s$ transition frequencies, not only when the laser input was tuned off resonance but also

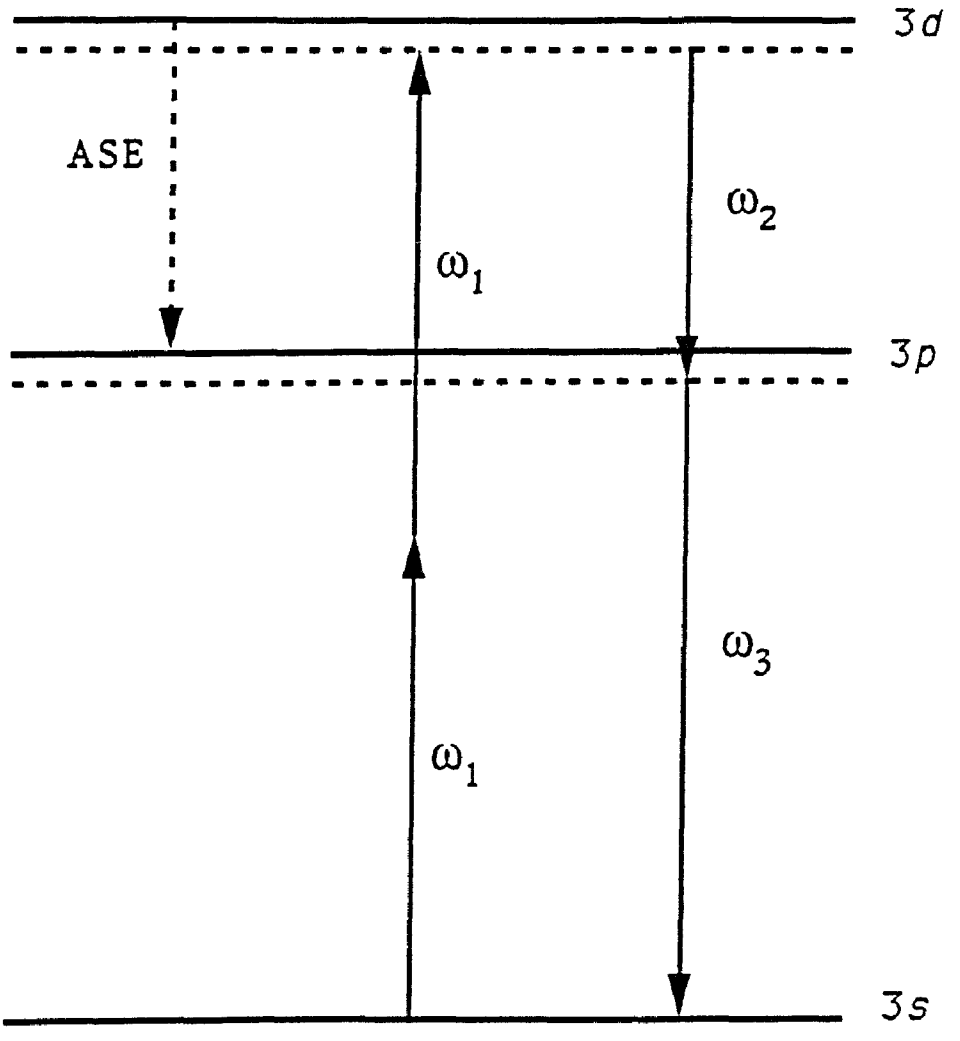

Figure 2.3. Energy-level diagram showing four-wave mixing and amplified spontaneous emission in sodium

when the laser was tuned precisely to resonance. When the laser is tuned to resonance, population can be transferred to the $3d$ level, inverting it with respect to the $3p$ level and leading to amplified spontaneous emission at the $3d \longrightarrow 3p$ transition frequency. Under conditions of intense resonant excitation, the gain of the amplified spontaneous emission process calculated in the absence of competition is many orders of magnitude larger than that of the four-wave mixing. However they found that for appropriate focusing of the laser beam only four-wave mixing is present. When the four-wave mixing process is inhibited through the use of counterpropagating pump beams, the normal result of amplified spontaneous emission is observed. They interpret these observations to be a consequence of a previously unrecognized competition between the amplified spontaneous emission and the four-wave mixing processes. The fields generated by the four-wave mixing process create a new pathway connecting $3s$ and $3d$ levels. This pathway can interfere destructively with that involving only the frequency of the incident field, prohibiting the transfer of population to the $3d$ level. Their work demonstrates that competition effects can occur under conditions more general than those previously believed to be necessary. They also studied amplified spontaneous emission and four-wave mixing when the laser was tuned to $4d$ level and found that strong competition did not exist under their experimental conditions. The gain cross section for the amplified spontaneous emission involving the $4d \longrightarrow 4p$ transition is nearly one order of magnitude larger than that for the $3d \longrightarrow 3p$ transition. It is believed that the fields generated by the four-wave mixing, which provide a new pathway connecting $3s$ and $4d$ levels, can not grow rapidly enough to suppress the amplified spontaneous emission

when its gain is sufficiently large.

This interference and the interaction involving two-photon absorption and two-photon resonant sum frequency generation [12] mentioned previously are related to each other in that they both involve a two-photon resonantly enhanced third-order nonlinear process. The competition between amplified spontaneous emission and four-wave mixing appears to result from the dependence of the amplified spontaneous emission on the population of the two-photon resonant state and the suppression of the two-photon transition moment by the presence of the fields generated by four-wave mixing process. This suppression of the population of the intermediate state is very similar to that described previously in the case of the three-photon resonance. This same effect may also be responsible for suppression of the intermediate state population in two-photon resonant sum-frequency generation. Since the atoms which have been excited to the intermediate resonant state are not available to participate in the sum-frequency generation process, suppression of this population leads to an enhancement of the intensity of the ultraviolet light generated by the nonlinear media. Thus a clear picture of this interference is needed to optimize the conditions under which this process takes place.

2.3 Interactions Involving Multiphoton Ionization and Stimulated Electronic Raman Scattering

Simultaneous multiphoton ionization and stimulated electronic Raman scattering in cesium vapor of wide pressure range were studied by J. A. D. Stockdale *et al*[13] (see Figure 2.4). At low vapor pressure multiphoton ionization occurs as a result of resonantly-enhanced laser excitation. At higher pressures where a strong signal of stimulated Raman scattering emission is observed near the $7p\,^2P$ and the $8p\,^2P$ levels, the multiphoton ionization shows a broadened peak in its excitation spectrum with a pronounced dip at the line center. A major contribution to the dip corresponding to the resonance frequency of the $7p\,^2P$ levels is due to an interference between the one-photon pathway and a three photon coherent process. The cancellation of a one-photon resonance is analogous to (but more complicated than) the interference between three-photon resonantly-enhanced multiphoton ionization and third-harmonic generation discussed earlier.

2.4 Some Other Works

Several other works related to these interference effects have appeared in the literature. M. Poirier[30] calculated the dependence of the ionization probability and third-harmonic intensity on the laser pulse duration (assuming a square pulse), gas pressure, detuning from resonance and laser intensity. His results are based on numerical solutions of a system of Bloch equations, and are in qualitative agreement with the results in xenon[5, 6].

R. N. Compton and J. C. Miller[31] observed the reappearance of the ionization rate through the $6s(3/2)^\circ$ J=1 resonance in Xe when a second laser,

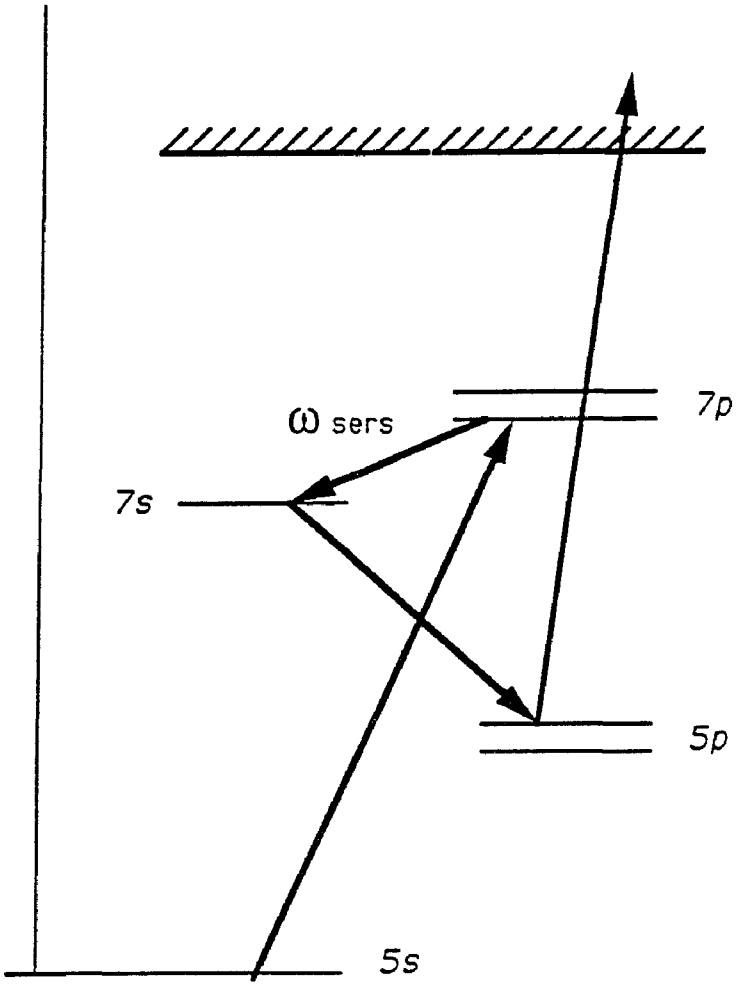

Figure 2.4. Energy-level diagram showing multi-photon ionization (MPI) and stimulated electronic Raman scattering in cesium.

which coupled the $6s(3/2)^{\circ}$ J=1 state to higher lying np and np' states, is applied to the atomic gas. S. P. Tewari and G. S. Agarwal[32] explained these results by considering the effect of the second laser field on the dispersion and phase matching conditions in the nonlinear medium. These authors were also able to explain the presence of third-harmonic generation to the long wavelength side of the $6s-6p$ transition in mercury[10].

More recently, W. R. Garrett *et al* [33] showed that the interference effect was completely effective in suppressing three-photon excitation of the 6s state of xenon when two separate lasers were used for the three-photon $2\omega_1+\omega_2$ pumping in a multiphoton ionization experiment involving three-photon excitation and four-wave mixing. The two lasers were independently pumped and had no phase relationship between them. When the two laser beams propagated colinearly in the same direction, the ionization signal disappeared. When counterpropagating geometry was used, the ionization signal was restored. Though the two laser fields are phase independent, the transition amplitude induced by the four-wave mixing is still coherent with the transition amplitude induced by three-photon excitation, they interfere each other and the net transition is suppressed. When the four-wave mixing is forbidden by the phase matching condition in counterpropagating geometry, the net transition reappears.

Theoretical[34] and experimental[35] reports of the effect of the addition of a buffer gas, dimer absorption and collisional dephasing processes on the third-harmonic generated and photo-ionization rate induced by an unfocussed laser beam nearly resonant with a three-photon transition in xenon have appeared. The last two papers have attempted to include the effect of the

bandwidth of the laser.

2.5 Phase Locking and Optical Balance

The earliest theoretical studies of the effects that intermediate resonances in nonlinear optical interactions would have on multiphoton absorption appeared in the Soviet literature. E. A. Manykin and A. M. Afanas'ev [36] considered, in 1965, the problem of the generation of light waves of frequency 3ω when light of frequency ω passed through a medium which had a characteristic transition frequencies in resonance with the frequency 2ω, (two-photon resonantly enhanced third-harmonic generation). They pointed out that as the amplitude of the third harmonic grew the nonlinear absorption (in particular, the two-photon absorption) of the first harmonic would decrease, so as to become equal to zero when a certain ratio of the two fields was reached. G. L. Gurevich and Yu. G. Khronopulo[37] considered parametric interaction of three intense electromagnetic fields with frequencies $\omega_3 = \omega_1 + \omega_2$ in a medium which has an resonance line at ω_3. They studied both frequency doubling and parametric frequency division. In their paper, they first introduced the concept of "phase locking". They showed that the rate of phase difference approaching towards π is much higher than the rate of the energy exchange between the fields when one of the fields is very weak. When the phase difference reaches π it will no longer change along the propagation and is "locked". This phase locking does not require that the phase matching condition $\Delta k = 0$, and the phase difference will tend to a value slightly different from π in case of a small phase dismatching. They also suggested that under certain conditions the second harmonic field will

propagate without absorption in a resonant medium that usually absorbs it. E. A. Manykin and A. M. Afanas'ev[38] later pointed out the possibility of making a medium transparent by multiphoton resonance. They showed that a coherent superposition of waves with different frequencies will move in the medium without absorption loss if a number of conditions are satisfied : 1) the transition amplitudes of two pathways are equal ; 2) the two pathways are 180° out of phase ; and 3) $\Delta k = 0$. They also pointed out that this suppression of absorption is mainly a consequence of the corresponding phase relations between the waves and totally different from the effect due to saturation.

These early theoretical papers preceded the development of tunable lasers. Such lasers, in particular, the dye lasers, led to practical experiments in resonantly enhanced nonlinear optical processes. The experimental results brought the importance of the phenomena to the attention of scientific community and stimulated further experimental and theoretical work. However the early Soviet papers were not recognized, at first, as providing an explanation to the experimental discoveries of the "competition" phenomena. J. J. Wynne independently did some theoretical work before he realized these Soviet studies. These competition phenomena have been attracting a lot of interest recently because of the apparent generality of its occurrence. J. J. Wynne[39] has shown theoretically that under the conditions of experimental observations, these two transition routes tend to balance each other, equal in magnitude and opposite in phase, so that complete cancellation of the ionization signal results. He proposes that the nonlinear optical balance described previously for the competition between third-

harmonic absorption and three-photon absorption is quite general. He thinks that it is related to a more general principle which he calls "law of minimum dissipation". Any deviation from the optical balance will increase the loss and the loss will bring the fields back to balance. As the light waves propagate through the lossy nonlinear optical medium, the wave amplitudes and phases will evolve so as to minimize dissipation. In case of three-photon resonantly enhanced third-harmonic generation, the distance to reach optical balance, from the initial condition $E_{3\omega} = 0$, is the linear absorption length for the third-harmonic field at 3ω. When perfect balance is achieved, any attempt to detect a population of the excited state, by ionization, fluorescence, or collisional transfer to another state, will fail, because there is no population at all. W. R. Garrett[40] has made comparisons between different theoretical approaches used in treating the same underlying physics, and between the predictions and the available experimental results of the phenomenon for three-photon and five-photon induced processes.

2.6 Theoretical Study of Coherent Control in Chemical Reactions

Recently developments in theoretical study in chemistry has been made in an area closely related to our interference experiments.

Manipulating the yield of chemical reactions is at the heart of chemistry, and controlling reactions by using laser lights has been a goal for decades. Early laser-based attempts at control relied either on the frequency resolution to locate a frequency which maximizes the desired yield, or on the use of high power lasers to alter the dynamics. These two major routes influenced the literature prior to 1985. Both methods suffer severe drawbacks ; the former,

mode selective approach, depends on the chance existence of a favorable branching ratio and the latter requires extremely high powers unmanageable in the laboratory [41]. Recently P. Brumer, M. Shapiro *et al* have proposed an approach for actively controlling the product distribution of chemical reactions using lasers[21, 22, 23, 24, 25, 26], which is based upon coherent paths and their interferences. Suppose that there are two simultaneous coherent paths to get to the chemical reaction products, the probability of producing a certain product will depend not only on each of the paths but also on their interference. Thus if one can design an experiment scenario such that by varying laboratory parameters one varies the interference condition, then one gets control over product distributions and product yields. They term this overall approach, which relies upon coherence and the use of interference between a minimum of two paths, coherent radiative control. They implemented these general principles in a number of examples, such as one-photon dissociation of a superposition state[21, 22, 23], control of photocurrent directionality through multi-frequency phase-coherent laser excitation[42], control of unimolecular reaction with two laser short pulses[43], and control of branching ratio by varying the elliptical polarization of the exciting laser[25]. In the last case, they showed that active control over differential cross section can be obtained with a single laser frequency of variable elliptical polarization. Dissociating the molecule via two orthonormal components of the polarization vector acts as the two simultaneous coherent paths and the interference between them provides the way to control. Their computational results showed that the interference term could be manipulated to give a vast range of possible control. The case most similar to our interference experiment is

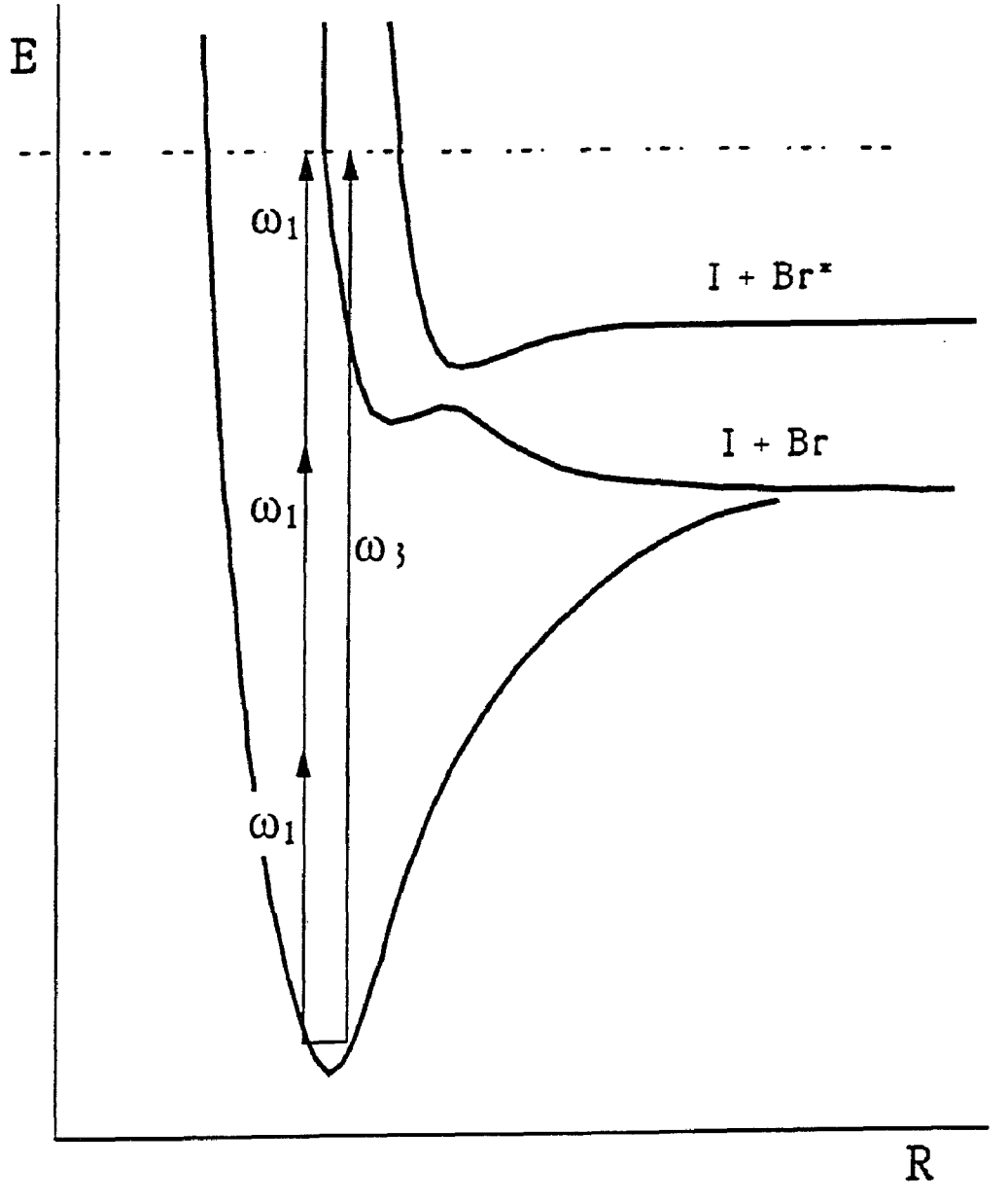

Figure 2.5. Schematic diagram of IBr potential curves showing one-photon and three-photon induced dissociation.

the control of unimolecular reaction through ω and 3ω excitation [24]. Excitations with the ω field and 3ω field provide the two simultaneous paths to the dissociation products and control of the branching ratio can be obtained by varying the phase difference of the two fields $\theta_3 - 3\theta_1$ and the ratio of the two laser amplitudes. They also gave an example by using IBr as the sample reactant[20], (see Figure 2.5), and showed that it is possible to vary the yield of excited state Br* atoms over a range of 25% - 95%.

They take our interference experiment of multiphoton ionization in mercury, reported in this thesis, as the first laboratory demonstration of coherent control over a process[44], although ours is not a chemical reaction, the experimental method and the underlying mechanism are closely related.

CHAPTER 3

THEORETICAL CONSIDERATION

3.1 One-Photon and Three-Photon Transitions

The effect of a multi-frequency laser field on the net transition moment for absorption by an atom into an excited state can be understood through the following discussion based on a time dependent perturbation formulation. As an example, we consider the interaction of third-harmonic generation and multiphoton ionization in which three-photon absorption and one-photon absorption are involved simultaneously.

When the third-harmonic radiation at frequency 3ω is incident upon an atom, it can be absorbed linearly by the atom, exciting the atom from the ground state $|1>$ to the upper state $|2>$, (see Fig. 3.1). The transition rate can be calculated using lowest-order time-dependent perturbation theory, and is given by:

$$W_1 = \frac{2\pi}{\hbar^2} \mid \mu_1 E_1 \mid^2 g(\Omega_{21} - 3\omega), \tag{3.1}$$

where μ_1 is the single-photon dipole transition moment, E_1 is the amplitude of the third-harmonic radiation field at 3ω, and $g(\Omega_{21} - 3\omega)$ denotes the frequency response of the atom. The transition frequency is related to the energy difference between the atomic excited and ground states by $\Omega_{21} = \frac{1}{\hbar}(E_2 - E_1)$. The transition rate, which is proportional to the intensity

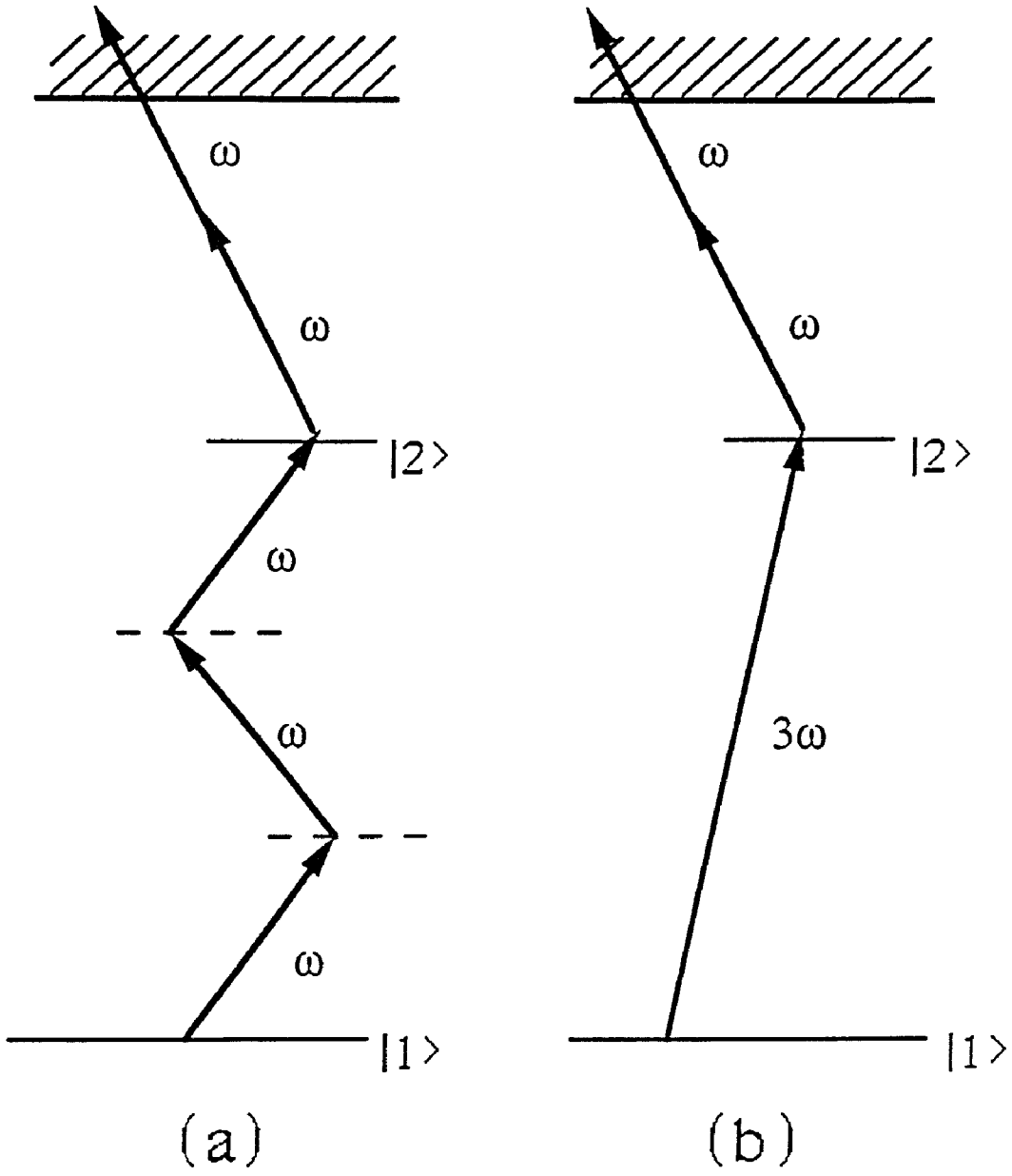

Figure 3.1. Schematic diagram showing: (a) three-photon absorption and (b) single-photon absorption in multiphoton ionization process. The dashed lines in (b) denote atomic virtual states of the atom.

of the radiation, reaches a maximum when the frequency of the radiation is equal to the transition frequency of the atom. This expression for the linear absorption rate is valid for weak fields, such that saturation effects are not present. The transition rate is independent of the phase of the radiation, since it varies as the modulus squared of $\mu_1 E_1$.

The atom can also interact with the fundamental field at frequency ω which is approximately one-third of the transition frequency of the atom,

$$3\omega \approx \Omega_{21} \quad . \tag{3.2}$$

The atom may absorb the radiation by a three-photon process. The absorption rate for this process may also be calculated using time-dependent perturbation theory (carried to third order) and is given by:

$$W_3 = \frac{2\pi}{\hbar^2} \left| \sum_{mn} \frac{(\mu_{2m} E_2)(\mu_{mn} E_2)(\mu_{n1} E_2)}{\hbar(\Omega_{m1} - 2\omega)\hbar(\Omega_{n1} - \omega)} \right|^2 g(\Omega_{21} - 3\omega) \quad , \tag{3.3}$$

where E_2 is the amplitude of the fundamental field, $\Omega_{i1} = \frac{E_i}{\hbar} - \frac{E_1}{\hbar} - i\Gamma_{i1}/2$, $\Gamma_{i1}/2$ are the linewidths of the transitions, and $g(\Omega_{21} - 3\omega)$ is the frequency response, or simply,

$$W_3 = \frac{2\pi}{\hbar^2} \left| \mu_3 (E_2)^3 \right|^2 g(\Omega_{21} - 3\omega) \quad , \tag{3.4}$$

where μ_3 is the effective transition moment for the three-photon absorption. This three-photon absorption rate varies as the cube of the field intensity, ${I_2}^3$, and can be resonantly enhanced if there is an intermediate state whose transition frequency from the ground state is near to the optical frequency or twice the optical frequency. The expression for the three-photon absorption rate is valid when the field strength, E_2, is less than that necessary for

saturation, and when the intermediate states are far enough from resonance that they are not populated directly by the radiation. Since the atomic levels are not usually appropriately spaced, the latter of these restrictions is not often encountered. The transition rate for this process is independent of the phase of the radiation, just as for the linear absorption process.

3.2 Ionization Rate for Two-Frequency Plane Wave Excitation

The single-photon and three-photon absorption processes described above are well understood individually. The possibility of an interesting effect arises when the atom is allowed to interact with both of the third-harmonic field E_1 and the fundamental field E_2, simultaneously. The atom can be excited to the state $|2>$ by a linear interaction or by a three-photon interaction. In this case, these two processes can not be treated separately and the above expressions for transition rates of one-photon absorption and three-photon absorption are no longer adequate. Instead we can consider it as an interference between two different, but coherent pathways [1]. Then the total transition rate will become:

$$W_{1,3} = \frac{2\pi}{\hbar^2} \left| \mu_1 E_1 e^{i\Phi_1} + \mu_3 (E_2 e^{i\Phi_2})^3 \right|^2 g(\Omega_{21} - 3\omega) \quad . \tag{3.5}$$

In other words, transition amplitudes are summed first, and then squared to give the transition rate, a proper way to treat coherent processes. The phase Φ_i ($i = 1,2$), of each field is not omitted in this expression since the relative phase can be extremely important. The single-photon and three-photon transition amplitudes can be matched by adjustment of the field amplitudes E_1 and E_2. Under this condition, the transition rate is

$$W_{1,3} = 2W_1[\,1 + \cos(3\Phi_2 - \Phi_1)]\ . \tag{3.6}$$

The importance of the relative phase $(3\Phi_2 - \Phi_1)$ is shown here since the transition rate will vary from four times the transition rate resulting from the interaction of the atom with the field E_1 when the amplitudes are in phase, to zero when the amplitudes are 180° out of phase. If the transition amplitudes due to interactions with the two fields are not of equal magnitude, the interference is still present, but the depth of modulation is reduced.

The discussion of the effect has been specifically for the interference between three-photon absorption and one-photon absorption, although similar arguments can be presented for the other interference phenomenon as well.

The interference between the transition moments involved in this work can be observed through resonantly enhanced multi-photon ionization, which does not require direct population in the upper state. In case that the upper state is populated, the interference can be observed through two different optical techniques. After excitation of the atomic system through the absorption of the radiation, the population of the excited state can be determined by 1) detecting the resultant fluorescence radiation, or 2) field ionizing or photoionizing the excited state atoms and detecting the net ionization current using simple biased collecting electrodes. Both techniques yield signals proportional to the population of the excited state. The interference should also be observable through the intensity of the transmitted radiation. By changing the phase of one of components of the radiation, the absorption of both components should be changed.

Here we only discuss the photoionization which we used in our experiment. In case of photoionization, the atom may be ionized by absorbing one (four-photon ionization) or two (five-photon ionization) additional photons of the fundamental field, and the total ionization rate for five-photon ionization can be given according to Fermi's Golden Rule:

$$W_{ion} = \frac{2\pi}{\hbar^2}\rho(5\omega)\left|\sum_m \frac{(\mu_{fm}E_2)(\mu_{m2}E_2)}{\hbar(\Omega_{m1}-4\omega)\hbar(\Omega_{21}-3\omega)}\right|^2 \times$$

$$|\,\mu_1 E_1 e^{i\Phi_1} + \mu_3 (E_2 e^{i\Phi_2})^3\,|^2 \quad , \tag{3.7}$$

where E_2 is the amplitude of the fundamental field, E_1 is the amplitude of the third-harmonic field, and $\rho(5\omega)$ is the density of the states in the continuum. This equation represents the ionization rate for five-photon ionization resonantly enhanced through state $|2>$. It does not require that the state $|2>$ is directly populated. It holds as long as the main contribution to the ionization comes from the resonant enhance through state $|2>$. In either case, whether state $|2>$ is populated or not, the interference should be observable.

Since the observation of the interference does not depend on whether state $|2>$ is directly populated or not, this multi-photon ionization can be effectively regarded as, for the simplicity in discussion, a "two-step" process which includes ground-to-excited transition and excited-to-continuum ionization. The first step is a third-order process relative to the fundamental field while the second step is a first-order one (for four-photon ionization) or a second-order one (for five-photon ionization). The cross section for the higher-order process usually is much smaller than that for the lower-order process. We may continue our discussion as if that the second step is saturated under the high laser intensity necessary for practical observation of

the multi-photon ionization. It leads to:

$$W_{ion} \propto | \mu_1 E_1 e^{i\Phi_1} + \mu_3 (E_2 e^{i\Phi_2})^3 |^2 \quad . \tag{3.8}$$

3.3 Ionization Rate for Two-Frequency Gaussian Field Excitation

Let us now derive an expression for the multi-photon ionization rate under laser beam excitation. The complete expression for the lowest-order

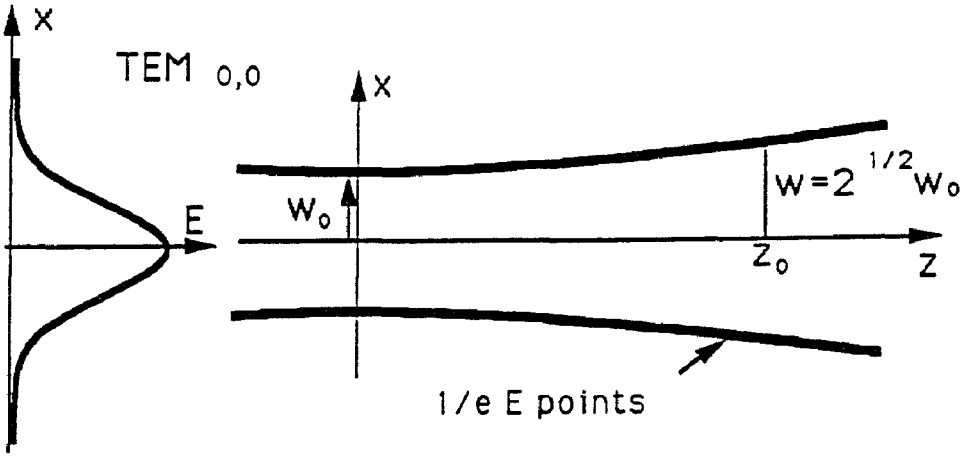

Figure 3.2. The lowest-order Gaussian mode, $TEM_{0,0}$.

Gaussian beam, $TEM_{0,0}$ mode, propagating along the z axis can be given as:

$$E(x,y,z) = \frac{E\, w_0}{w(z)} \exp\left[-\frac{r^2}{w^2(z)}\right] \exp\left\{-i\left[kz - \phi - \tan^{-1}\left(\frac{z}{z_0}\right)\right]\right\}$$

$$\times \exp\left[-i\frac{kr^2}{2R(z)}\right] \tag{3.9}$$

where E is the field amplitude on the beam axis at the focus ($z = 0$) and k is the propagation constant. The "spot size" w(z), defined as the $1/e^2$ intensity beam radius, varies along z axis as:

$$w(z) = w_0\left[1 + \left(\frac{z}{z_0}\right)^2\right]^{1/2}, \tag{3.10}$$

where $w_0 = w(0)$ is the minimum "spot size", named beam waist radius. The scale factor z_0, defined as:

$$z_0 = \frac{\pi w_0^{\,2}}{\lambda}, \tag{3.11}$$

is one half of the confocal parameter. The radial phase factor of $\exp\left[-i\frac{kr^2}{2R(z)}\right]$ in Equation 3.9, which represents the spherical characteristic of the wave front of a Gaussian beam, will be omitted for simplicity later. This radial phase factor will be automatically cancelled in the relative phase of the two transition amplitudes if the wave fronts of the two fields are matched and the phase matching condition, $\Delta k = 0$, is satisfied. These two conditions are required by this interference experiment anyway and will be discussed in detail in the following sections. In fact, the relative phase due to radial phase factor at $z = \pm z_0$, where R(z) is minimum, is about $\frac{\Delta k\, r^2}{4z_0}$ which is much smaller than the relative phase due to Δk itself. Thus the radial phase factor can be ignored even if the phase matching condition is not satisfied.

From Equation 3.10, it is easy to see that the "spot size" w(z) varies along the z axis, thus the field amplitude of the beam has to vary accordingly as required by energy conservation law. The variation of the field amplitude along the beam axis will be shown explicitly if we change Equation 3.9, by

using Equation 3.10, into :

$$E(x,y,z) = \frac{E}{\left[1+(\frac{z}{z_0})^2\right]^{\frac{1}{2}}} \exp\left[-\frac{r^2}{w^2(z)}\right] \exp\left\{-i\left[kz - \phi - \tan^{-1}(\frac{z}{z_0})\right]\right\} .$$

..... (3.12)

When we simply replace the two fields $E_1 e^{i\Phi_1}$ and $E_2 e^{i\Phi_2}$ in Equation 3.8 by two $TEM_{0,0}$ Gaussian fields expressed in the form of Equation 3.12, the multi-photon ionization rate becomes:

$$W_{ion} \propto \left| \frac{\mu_1 E_1}{\left[1+(\frac{z}{z_{01}})^2\right]^{\frac{1}{2}}} \exp\left[-\frac{r^2}{w_1^2(z)}\right] \exp\left\{-i\left[k_1 z - \phi_1 - \tan^{-1}(\frac{z}{z_{01}})\right]\right\} \right.$$

$$\left. + \frac{\mu_3 E_2^3}{\left[1+(\frac{z}{z_{02}})^2\right]^{\frac{3}{2}}} \exp\left[-\frac{3\,r^2}{w_2^2(z)}\right] \exp\left\{-i3\left[k_2 z - \phi_2 - \tan^{-1}(\frac{z}{z_{02}})\right]\right\} \right|^2 .$$

..... (3.13)

Note that E_1 and E_2 are field amplitudes on the beam axis at the waists and the subscripts 1 and 2 denote the third harmonic field and the fundamental field, respectively.

Equation (3.13) provides us a mathematical expression for our interference experiment. Based upon it, we are going to discuss some very important conditions to carry out the experiment in the next section.

3.4 Considerations on Preconditions for Interference Experiment

The main goal of this project is to study interference between two optical processes. We should find ways to control the relative phase externally, match the two amplitudes and their wave fronts and maintain the amplitude and phase relation in the whole interaction region to a certain degree such that the interference is observable.

Let us look back for a while to see what we did physically in those mathematical derivations. Up to now we have already made a couple of presuppositions. First the two fields should be highly coherent. The coherence of the fields are extremely important. If the two fields were not coherent to each other it would not make any sense when we add the two transition amplitudes before squaring. The coherence is implied when we say one field is the third harmonic of the other. The third harmonic generation process usually maintains a very good phase relation with the fundamental field[45]. Second, $TEM_{0,0}$ mode has been used to represent Gaussian fields. We may see later that the $TEM_{0,0}$ mode is definitely a preference, if not a necessity, comparing with higher-order Gaussian modes. Third, by representing the two fields in the same form of mathematical expression in the same coordinate system, we have assumed that the two fields propagate colinearly in one direction (transverse overlap) and their beam waists are located at a same spot $z = 0$ (longitudinal overlap). These two overlaps are not only good in simplification of mathematical expression but also physically essential in this experiment.

From Equation 3.13, several other important points can be drawn. We know that the depth of modulation of the interference is maximized when the

two transition amplitudes are matched everywhere. We can adjust the intensity ratio of the two fields to match the transition amplitudes at a certain spot, but to keep them matched everywhere we have to design a common spatial dependence for them. Transversely it requires that the two beam waist radii satisfy the relation,

$$w_{02} = \sqrt{3}\, w_{01} \ . \tag{3.14}$$

Note that the confocal parameters of the two fields are equal under the condition of Equation 3.14 since $\lambda_2 = 3\,\lambda_1$ (see Equation 3.11). We have:

$$z_{01} = z_{02} \ , \tag{3.15}$$

and may simply call it z_0 since we need no longer to distinguish it for the two fields. This also implies that the two fields will have the same radius of curvature R(z) for their wave fronts, because the dependence of R(z) on z is solely determined by z_0 as:

$$R(z) = z[1+(\frac{z_0}{z})^2]. \tag{3.16}$$

The relation between the two beam waists of Equation 3.14 is automatically satisfied if the 3ω field is generated by third harmonic generation process, because third harmonic generation is a third-order process and has an intensity dependence as I^3. From basic theory for Gaussian beams we know that the two fields with frequencies ω and 3ω will have, if the condition of Equation 3.14 is satisfied, same complex beam parameters q, defined as:

$$\frac{1}{q(z)} = \frac{1}{R(z)} - i\,\frac{\lambda}{\pi n w^2(z)}. \tag{3.17}$$

The complex beam parameters of the two fields will change but remain equal to each other as the two fields propagate through a non-dispersive optical

system following the ABCD law. Thus we expect Equation 3.14 to hold even if we refocus the two beams by a non-dispersive optical system after the third harmonic generation process. We have for the whole interaction region, according to Equation 3.10,

$$w_1(z) = \frac{w_2(z)}{\sqrt{3}} \quad . \tag{3.18}$$

That means the two transition amplitudes follow the common transverse factor $\exp\left[-\frac{3\,r^2}{w_2^2(z)}\right]$.

By using Equation 3.18 and combining the phase factors to make it simpler and easier to discuss the phase relations between the two transition amplitudes, we may rewrite Equation 3.13 as:

$$W_{ion} \propto \exp\left[-\frac{6\,r^2}{w^2(z)}\right]\left|\frac{\mu_1 E_1}{\left[1+(\frac{z}{z_0})^2\right]^{\frac{1}{2}}}+\frac{\mu_3 E_2^3}{\left[1+(\frac{z}{z_0})^2\right]^{\frac{3}{2}}}\times\right.$$

$$\left.\exp\left\{-i\left[(3k_2-k_1)\,z-(3\phi_2-\phi_1)-2\tan^{-1}(\frac{z}{z_0})\right]\right\}\right|^2 , \tag{3.19}$$

where w(z) is the "spot size" of the fundamental field and z_0 is half of the confocal parameter for both of the fields. Here we should notice that this equation for ionization rate is valid when the ionization step is saturated by the intense fundamental field. In case of focused beams, the intensity of the fundamental beam varies along the axis. The ionization step could be saturated within the focal region but will not be saturated away from it, then another factor of intensity dependence needs to be added to this equation for

places where the ionization step is not saturated.

But, longitudinally the two transition amplitudes vary differently along the axis, one varies as $\left[1+(\frac{z}{z_{01}})^2\right]^{-\frac{1}{2}}$ and the other as $\left[1+(\frac{z}{z_{02}})^2\right]^{-\frac{3}{2}}$. It is impossible to match the two amplitudes throughout the entire interaction region unless collimated beams are adopted. Then the confocal parameters are much greater than the physical size of the interaction region so that the transition amplitudes can be regarded as constant about z. It will also help in maintaining the relative phase by cancelling the effect of the $2\tan^{-1}(\frac{z}{z_0})$ term in the phase factor in Equation 3.19. Unfortunately the idea of using collimated beam is contradictory to the fact that a very high power density of laser field is required to carry out the nonlinear interaction. To date neither such a powerful laser system nor the optical components capable of handling the power density are available. We have to compromise and use a focused laser beam. Under this condition the transition amplitudes can be matched at, at most, two locations symmetrically placed about the focus and the $\tan^{-1}(\frac{z}{z_0})$ terms in the phase factors will cause a 2π phase shift in the relative phase from $-\infty$ to $+\infty$; or a π phase shift from $-z_0$ to $+z_0$, approximately the interaction region for the highly intensity dependent nonlinear process. The depth of modulation for the interference will be reduced but still observable because a large portion of ionization signal is generated at a very small region around the focus and the interaction is very weak away from the focus. This π phase shift of the focused Gaussian beam is the main obstacle to the establishment of a spatially independent relative phase between the two transition amplitudes and could severely affect the application of "coherent

control" in chemical reactions in the future except for those processes in which the $\tan^{-1}(\frac{z}{z_0})$ terms happen to be cancelled by each other. The interference involving four wave mixing and amplified spontaneous emission is one of the examples where $\tan^{-1}(\frac{z}{z_0})$ terms do not exist in relative phase. In processes that the $\tan^{-1}(\frac{z}{z_0})$ terms do exist, a possible way to survive is to make use of the difference of the propagating phase terms, $\Delta k\, z$, to compensate the dephasing effect of the $\tan^{-1}(\frac{z}{z_0})$ terms.

Although $\Delta k\, z$ could be used as a compensation in some cases, usually it will cause additional undesired shift in the relative phase. It should be maintained, at least approximately, $\Delta k = 0$, which is called phase matching condition. Phase matching condition is a very important concept in nonlinear optics. In many nonlinear optical processes, this condition needs to be met so that the field generated in the nonlinear medium is in phase with the nonlinear polarization and enhanced by cumulation. In the case of the interference experiment, we are also required to meet the phase matching condition because we want to keep the relative phase as uniform as possible throughout the entire interaction region such that the interference would not be averaged out. In Equation 3.19, $\Delta k\, z$ is represented by the difference between the propagating phase terms $3k_2 z$ and $k_1 z$. We should maintain, approximately, the phase matching condition:

$$3\, k_2 - k_1 \approx 0, \tag{3.20}$$

We use " $\approx$ " instead of " $=$ " because the optimum usually does not appear at exactly $\Delta k = 0$ in nonlinear optical processes using focused laser beams.

For example, it is required that Δk be slightly greater than 0 to compensate the $\tan^{-1}(\frac{z}{z_0})$ terms and get efficient third harmonic generation when a focused laser beam is used [45].

The strong absorption of the third harmonic field at resonance is another concern. This prevents us from generating harmonics when the the fundamental laser field is tuned to exactly one third of the transition frequency. Thus a certain amount detuning of the laser field from resonance is necessary. In our experiments, the amount of detuning is determined by the maximum efficiency in third harmonic generation without any consideration on compensation of the $\tan^{-1}(\frac{z}{z_0})$ terms in the area where we observe the interference.

Lasers do not always operate in $TEM_{0,0}$ mode and their output can be a higher-order mode or even a linear combination of several Gaussian modes. The expression for $TEM_{m,n}$ mode is given by:

$$E(x,y,z) = \frac{E\, w_0}{w(z)} H_m\Big[\frac{2^{\frac{1}{2}} x}{w(z)}\Big] H_n\Big[\frac{2^{\frac{1}{2}} y}{w(z)}\Big] \exp\Big[-\frac{r^2}{w^2(z)}\Big]$$

$$\times \exp\Big\{-i\Big[kz - \phi - (1+m+n)\tan^{-1}(\frac{z}{z_0})\Big]\Big\} \exp\Big[-i\frac{kr^2}{2R(z)}\Big] \quad (3.21)$$

where all symbols, $w(z)$, w_0, and z_0 are as defined previously. E is an amplitude constant and it is not so easy to interpret it further as we did for the $TEM_{0,0}$ mode. The symbol $H_n(u)$ stands for the Hermite polynominal of order n and argument u. It is instructive to consider a few of the lower-order ones:

$$H_0(u) = 1$$

$$H_1(u) = 2\,u$$

$$H_2(u) = 2\,(u^2 - 1)$$

There is a great deal of similarity between Equation 3.21 and 3.9; the radial phase factor is the same, the exponential variation with $r^2 = x^2 + y^2$ is the same, and the multiplying factor $w_0/w(z)$ is the same. But there are differences.

First note the phase shift in z direction is dependent upon the mode number m and n. The $2\tan^{-1}(\frac{z}{z_0})$ term in the relative phase of Equation 3.19 becomes $4\tan^{-1}(\frac{z}{z_0})$ for $TEM_{1,0}$ mode, $6\tan^{-1}(\frac{z}{z_0})$ for $TEM_{2,0}$ mode and so on, dephasing gets faster and faster.

For large x or y, the exponential behavior still dominates and thus the field is tightly bound to the z axis like a "beam". But at small x (or y), the field is modified considerably by the polynominals and forced to zero at some points. Hence we will see $(m + 1)(n + 1)$ "dots" in a $TEM_{m,n}$ mode beam pattern. Unlike $TEM_{0,0}$ mode, the higher-order modes do not have a uniphase wave front surface. The field of higher-order modes reverses the direction when acrossing the "zeros" (see Figure 3.3), thus there is a 180° phase difference between the fields of two adjacent "dots". Within each "dot", the equi-phase surface has the same spherical curvature as the $TEM_{0,0}$ mode.

It is obvious that multi-transverse-mode (a linear combination of several $TEM_{m,n}$ modes) laser operation is not adequate for any phase sensitive processes. The wave fronts of different modes overlap with each other but

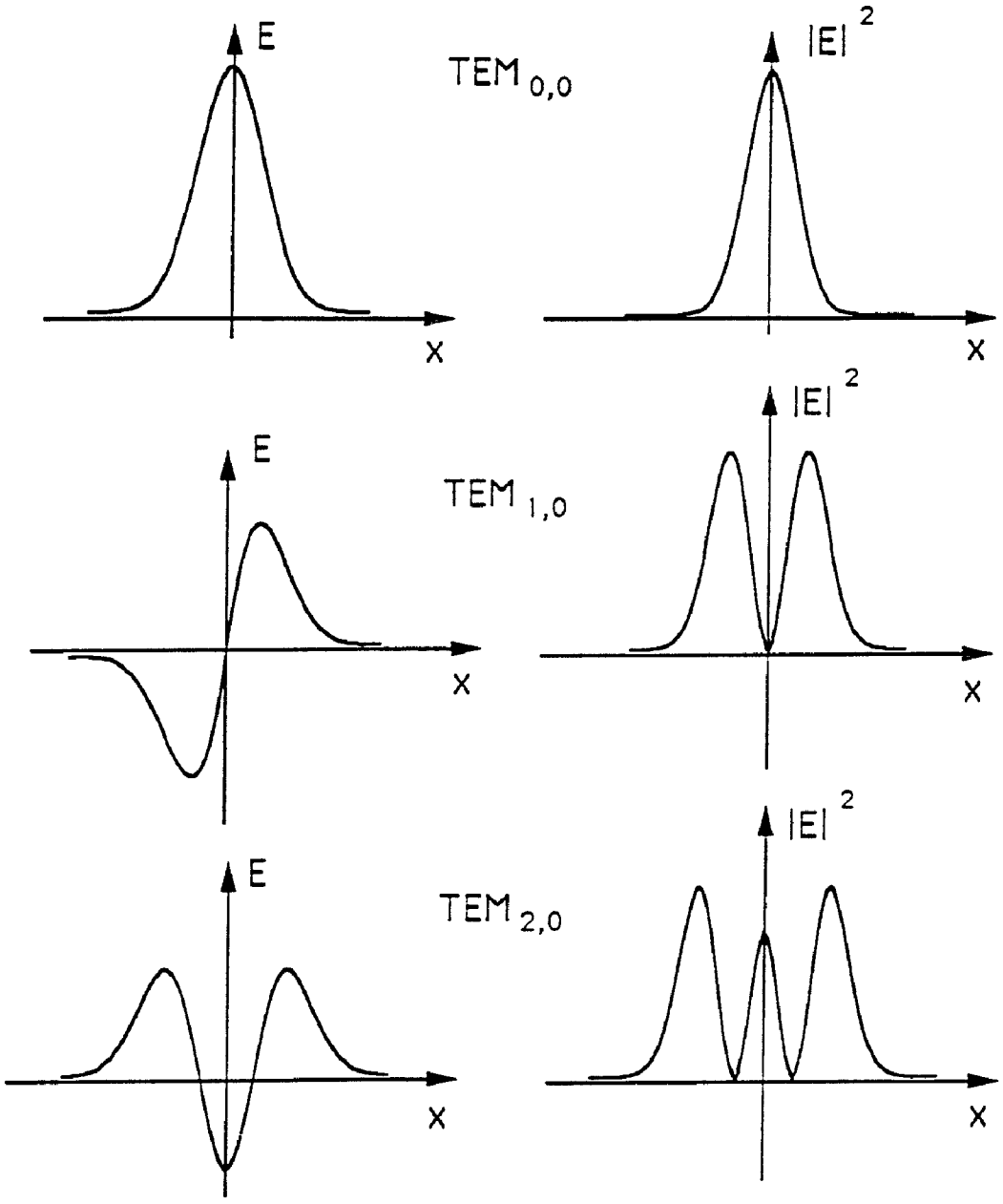

Figure 3.3. The field E, and intensity $|E|^2$ of various Gaussian modes. Note that the fields reverse direction for higher-order modes.

their phase could be very different. It is hard to imagine that any observable interference exists under multi-mode laser excitation. For single-transverse-mode operation at a higher-order $TEM_{m,n}$ mode, the disadvantages are as following. First the focal spot will be larger than that of a $TEM_{0,0}$ mode such that a tighter focusing or higher power laser beam is required to provide same power density for the nonlinear optical process. Second and more important point is the complexity of the phase of the higher- order mode longitudinally as well as transversely. Theoretically it could be possible to use a higher-order mode laser beam for the interference experiment in which the $\tan^{-1}(\frac{z}{z_0})$ terms in phase factors cancel each other. But practically it would be much more difficult, if still possible, to do phase sensitive experiments with higher-order $TEM_{m,n}$ mode excitation because we need "dot-to-dot" overlap instead of merely a "beam-to-beam" overlap.

The term of phase difference $(3\phi_2 - \phi_1)$ is a constant in Equation 3.19 and is determined by initial conditions. This is the key factor which we can control externally in our multi-cell design for this experiment. This external phase control provides us the opportunity to study the interference by directly observing the phase dependence of ionization and makes this experiment significant.

As a summary, those points discussed above are listed as following:

1. coherent fields
2. $TEM_{0,0}$ mode laser operation
3. transverse and longitudinal beam overlap
4. transition amplitude matching
5. phase matching

6. highly non-dispersive optical system except for that of phase control

7. detuning

8. external phase control

To fulfill these preconditions was the main tasks in carrying out this experiment. Some of them turned out to be trivial but others quite challenging.

CHAPTER 4

OUTLINE OF EXPERIMENT SETUP

4.1 Introduction

Various atomic vapors can be used for the observation of these interference effects. We used the $6s\,^1S_0 \rightarrow 6p\,^1P_1$ transition of mercury for the study of the interference between three-photon and single-photon absorption. Suppression of the three-photon resonantly-enhanced five-photon ionization rate was reported previously with this transition, as well as the generation of the third-harmonic radiation[10]. The competition involving multiphoton ionization and third harmonic generation has been studied intensely in noble gases and mercury vapor. We choose mercury as our sample material because the frequency of the transition in mercury is more convenient than those in the noble gases. The wavelengths of fundamental laser fields used in experiments of the noble gases are in the range of 320 nm to 440 nm, which is not the most convenient range to obtain high energy laser pulses from a dye laser system. Moreover the wavelengths of the third harmonic fields generated in noble gases are so short that very special optical components are required in the interference experiment if we choose noble gas as the sample. On the other hand, the fundamental laser field required for the three-photon resonance to the 6s to 6p transition in mercury is around 555nm. Using dye solution of rhodamine 6G in methanol, a pulsed dye laser pumped by second harmonic of YAG laser will operate efficiently at this wavelength.

The third harmonic generated in mercury is about 185 nm, which is not too difficult to handle. Optical components in this range are commercially available and relatively affordable.

In this chapter, we are going to report the setup for the interference experiment and the reasons for doing so. This experimental setup was used for the study of the interference between the 6s - 6p single-photon and three-photon transitions in mercury. However, a similar design can be used in various phase-controlled experiments. When describing the setup, we try to put it on a diversified base and use our mercury experiment only as an example.

Some details of the experimental setup related only to a specific experiment will be left to next chapter, in which we will report several experiments separately.

4.2 Experimental Cells

As reported in Chapter 3, there should be a means to control the relative phase in order to directly study the interference. In all the competition experiments reported before, the generation of the second field and the multi-photon ionization are carried out in the same region and the relative phase is not controllable. Thus a multi-cell design is necessary to separate the two processes and make the external control of the relative phase possible.

The experiment to observe the interference between various optical processes will involve the generation of a signal beam (be it the third-harmonic, or sum-frequency, or difference frequency) in one vapor cell, and the observation of the interaction of the nonlinear atomic vapor with the

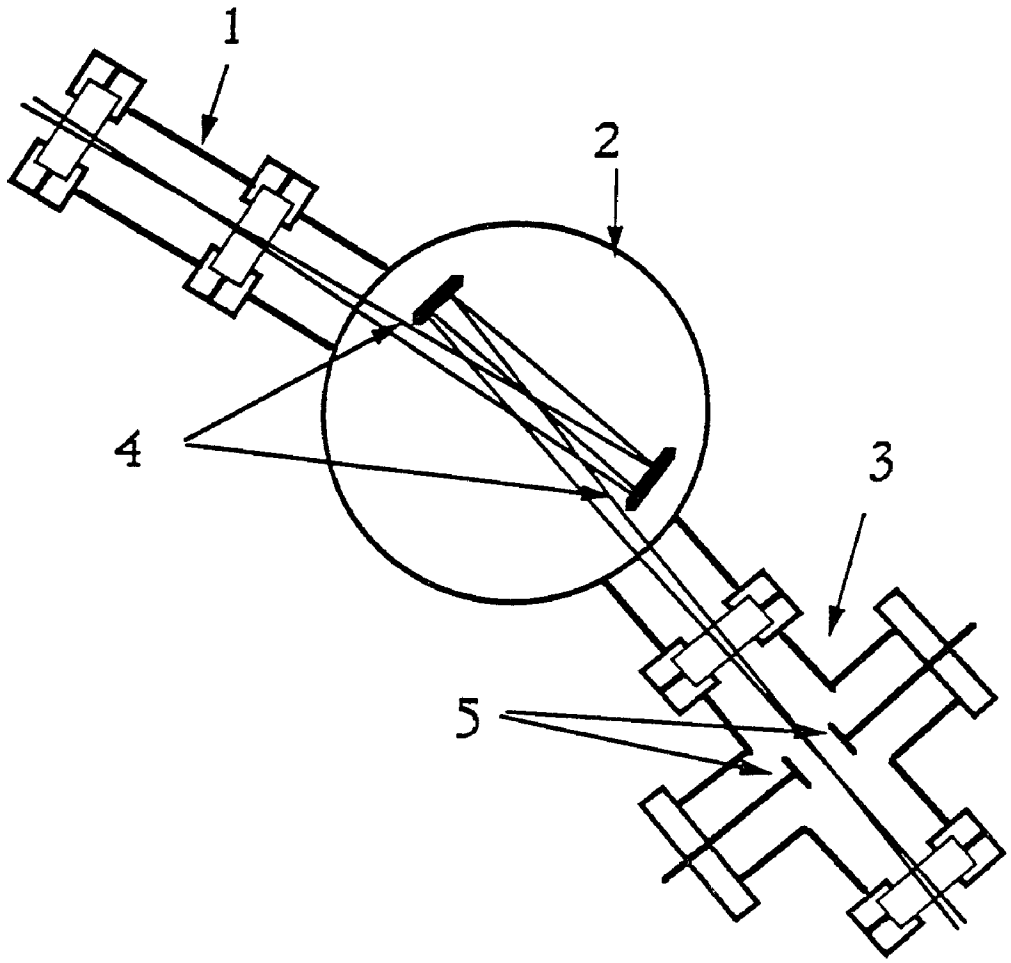

Figure 4.1. Schematic diagram for the experimental cells, (1) the generation cell, (2) the dispersion cell, (3) the interaction cell, (4) the mirrors and (5) the collecting electrodes.

multi-frequency field in another cell (see figure 4.1). In this way the two processes of nonlinear generation and multi-frequency absorption are separated, and the effect of the interference can be unambiguously determined. The relative phase of the fields can be controlled by inserting a third cell (dispersion cell), between the generation cell and the interaction cell.

The dispersion cell contains a nonabsorbing gas such as argon. Since argon, like any gas, is dispersive the phase delay of the various fields differs as they propagate through the dispersion cell. Changing the density of the argon gas delays the different fields by different amounts and thus changes the phase difference of transition amplitudes in interaction cell. In case of the experiment involving 6s - 6p resonantly enhanced multi-photon ionization in mercury, the change of the phase difference $(3\phi_2 - \phi_1)$ between the three-photon transition amplitude and that of one-photon transition at the interaction cell is determined by

$$\frac{\Delta(3\phi_2 - \phi_1)}{\Delta P} = \frac{3(n_2 - n_1)l\omega}{P_0 c} \tag{4.1}$$

where ΔP is the pressure change, n_2 , n_1 are refractive indices at 555 nm and 185 nm under standard condition STP, P_0 is the pressure of standard atmosphere and l is the path length of the beams in the dispersion cell. Since $(n_2 - n_1) = 4.5\times10^{-5}$ [46], and the l is about 50 cm, argon pressure changes as small as a few torr are sufficient for inducing a complete π phase shift between the interference terms, changing the absorption rate from a minimum to a maximum.

This technique of phase control of the harmonic radiation has been used previously in a number of "nonlinear interferometers". In these devices, the harmonic of the laser radiation is produced by two separated generators. The net harmonic signal, which depends on the interference between the two individual harmonic fields, varies as the optical path length difference between the fundamental radiation and the harmonic radiation is varied. This can be brought about, 1) by changing the gas density of a dispersive gas between the two generators, 2) by changing the distance between the two generators, 3) by applying a high-intensity laser field which modifies the refractive index through a nonlinear effect, or 4) by tuning the frequency of the laser through an optical resonance of atomic vapor in the region between the generators. In all of these cases, the phase difference between the laser radiation and the harmonic at the second generator is changed, thus changing the interference condition. These have been used for the measurement of the dispersion in refractive index[47,48] of various gases, the intensity-dependent refractive index in gases[49], and the oscillator strength of atomic transitions[50].

The quality of field coherence and the overlap of the wave-fronts of the two components of the field are very important in this experiment. Chromatic aberrations of lenses over the wavelength differences involved in this work preclude their use in the experimental setup after the generation cell. Instead two aluminized spherical mirrors (Acton 2000-1D-0.5M, enhanced for VUV wavelength, reflectance 88% at 185 nm, 92% at 555 nm) positioned as close to normal incidence as possible were used in the dispersion cell to focus the beams, which diverged from the generation cell, into the interaction cell. We used two mirrors with same focal lengths, 25cm, such that the incidence

angles at the two mirrors are as small as physically possible (approximately 3°) without blocking the beams. No significant astigmatism was observed under this condition.

The detailed construction of the generation cell and interaction cell is as shown in Figure 4.2. Both the two are vacuum sealed stainless steel cells with o-ring sealed windows. The main body of the generation cell is made from a piece of 1 inch diameter tubing about 10 cm long. On each end of the generation cell there is an ASA flange with o-ring groove for sealing the window. The window is clamped onto the ASA flange by another specially made flange also with o-ring groove such that the metal surfaces of the two flanges contact each other at the edge when they are bolted in place and a space is left at the center for the window and pressed Viton o-rings. The interaction cell is made of a six-way cross. The structure of the front window, rear window and the two side windows is much more the same as that of the generation cell. The two side windows, which are not shown in Figure 4.2, are used for inspecting the interaction region in this experiment and could be used as entrance ports if an additional laser beam is introduced to carry out the ionization step. The top and bottom ports of the cell, used to collect the ionization signal, are composed of "Del-Seal" flanges and electrical feed-throughs.

We use 1.5 inch diameter, 3/8 inch thick fused silica optical flats as the windows. The windows that the third harmonic field passes through are UV grade with a transmittance greater than 80% at 185nm. As mentioned previously, only a non-dispersive optical system can maintain the transverse and longitudinal overlap of the fundamental and third harmonic fields. But

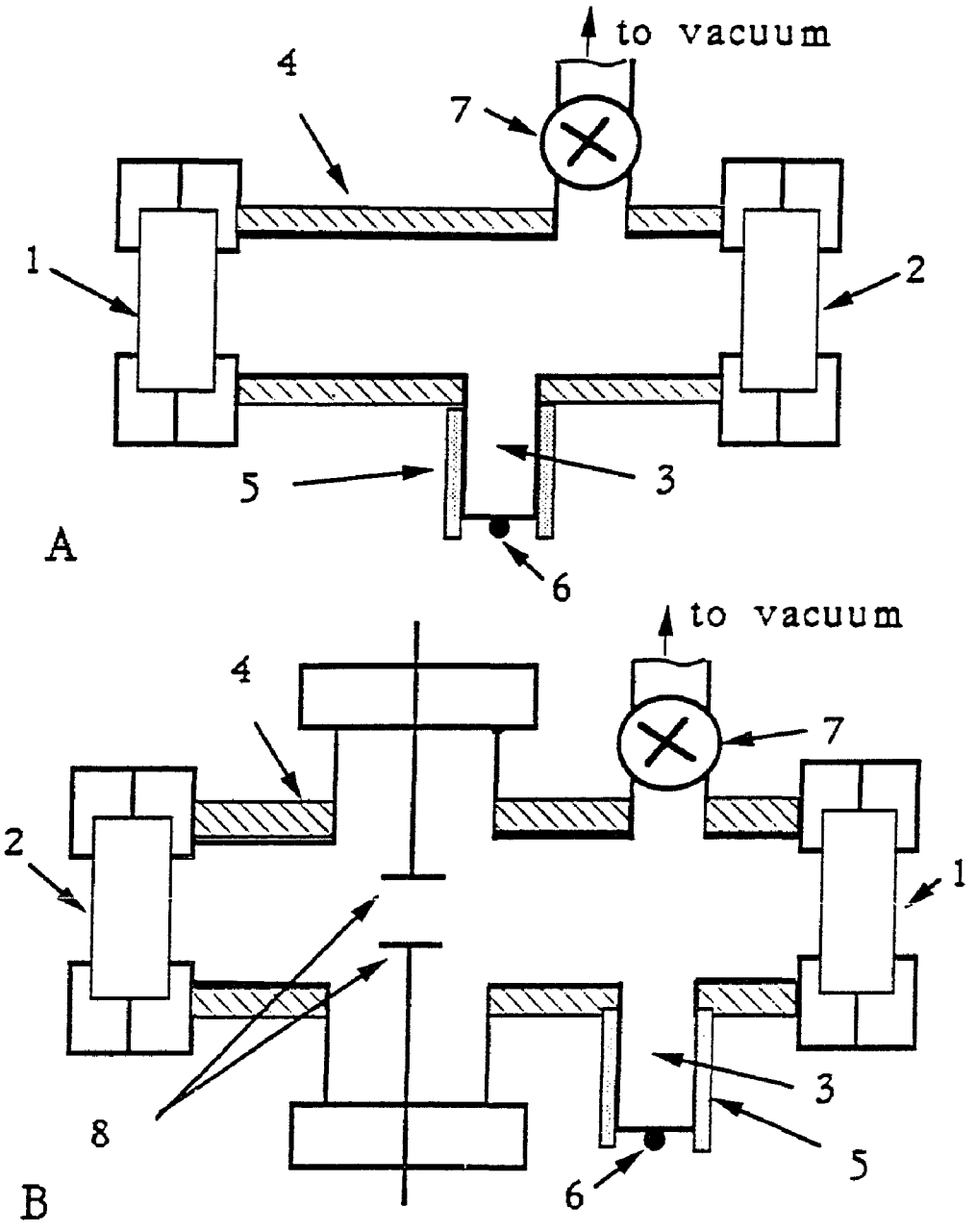

Figure 4.2. Schematic diagram of two mercury cells, (A) generation cell and (B) interaction cell: (1) windows, (2) parallel windows, (3) cold fingers, (4) heating tapes, (5) heating pads, (6) temperature sensors, (7) vacuum valves, and (8) collecting electrodes.

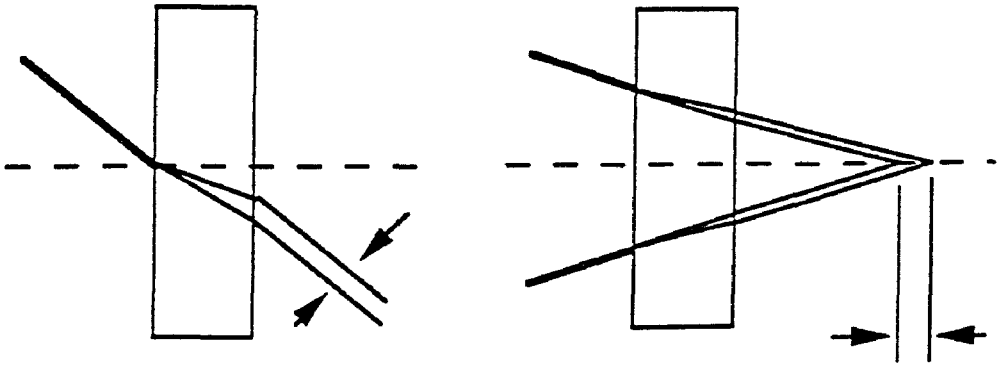

Figure 4.3. Effects of window on a multi-wavelength beam

fused silica is dispersive, and we have to have windows. A wedged window is like a prism. Under our experimental conditions, a typical general purpose window of a wedged angle of only 3 minutes will induce a 25μm deviation between beam axes of the two fields at the focus, where the beam waist of the fundamental field is about 25μm. Two parallel windows are used for the exit port of the generation cell and the entrance port of the interaction cell, to avoid the prism effect. Figure 4.3 shows two other effects of a window, present even if it is highly parallel. First it may cause a "walk off" of the two components of the field with different wavelength when the field is incident upon the window at an angle other than 0°. Under our condition, an incidence angle as small as 3° will induce a 25μm "walk off", the same size of the fundamental beam waist. Thus we carefully adjusted normal incidence at the two parallel windows during the interference experiment. Second it will

make the two components of a focused field focus at different distance. In our experiment, the fundamental field and third harmonic field diverged through the exit window of the generation cell and refocused through the entrance window of the interaction cell and the beam waists of the two fields are calculated to be 0.08cm apart. If we change the windows into a smaller aperture, we may use a thinner fused silica flat and retain the same physical strength. It will help to reduce the effects of the windows.

T (^{o}C)	- 28	- 8	16	45	81	125
P (torr)	10^{-5}	10^{-4}	10^{-3}	10^{-2}	10^{-1}	1

Table 4.1. Mercury vapor pressure as a function of temperature.

The mercury is condensed in the cold fingers of the generation cell and interaction cell. The vapor density in a closed system is determined, at equilibrium, by the coldest spot of the system. In our experiment, the two cells were kept heated by heating tapes to a temperature higher than that of the cold fingers. Outside the heating tapes, the cells are wrapped by aluminum foil to keep the temperature uniform because aluminum is a much better heat conductor than stainless steel. The cold fingers were heated by heating pads which were controlled by a home-made temperature controller. The cell body temperature, which has to be higher than that of the cold fingers, can not be set excessively high because the life time of Viton o-rings

will decrease as the working temperature increases and it decreases very fast as temperature gets higher than 90°C. The cold fingers are welded onto the cell bodies. The excessively high cell body temperature will cause higher cold finger temperature by conduction and leaves no room to control the cold finger temperature by controlled heating. We use two heating tapes for the interaction cell and one tape for the generation cell. We used tapes with low power per unit length such that the tapes are long enough to wrap all over the cells. The lower power heating pads and the proportional operation of the controller are designed to prevent overshooting in temperature control. Since the body temperature of the generation cell is more than 60°C higher than room temperature, some heat insulation cloth is wrapped around it. Attached to the cold finger of each cell are two temperature sensors. One of them, used for controlling the temperature of the cold finger, is a YSI 44007 precision thermistor with a resistance temperature coefficient 168Ω/°C at 30°C, and 19.9Ω/°C at 80°C. The other, used for monitoring the temperature of the cold finger, is a copper constantan thermocouple with a voltage temperature coefficient 0.04mV/°C at 30°C, and 0.045mV/°C at 80°C. Every time before we took data, we started to heat the cells four to eight hours earlier to make sure the temperature as well as the physical dimensions of the cells stablized. In a typical data taking period of about 2 hours the temperature fluctuation of the cold finger of the generation cell, whose temperature was set at about 80°C, was less than ±0.3°C; and the fluctuation of the interaction cell cold finger temperature, set around 30°C, was less than ±0.2°C. The importance of the stability of the cold finger temperature will be discussed later.

The mercury density in the generation cell was maintained at a relatively high level ($\sim$ 0.1 torr) for efficient generation of the third-harmonic field. The density dependence of the third-harmonic intensity has been reported in reference[10]. Control of the density of mercury in the generation cell will determine the intensity of the third-harmonic radiation, providing a simple means of matching the one-photon and three-photon transition amplitudes for this interference process. Due to phase matching conditions, the peak of the excitation spectrum of the third-harmonic is at a shorter wavelength, 554nm, than the mercury transition wavelength, 555nm. This detuning also corresponds to the peak of the multiphoton ionization signal as determined by D. Normand, *et al*,[10], and observed in our own experiment. The third-harmonic radiation under 1 nm detuning is still quite close to the resonance, hence we examined the effect of the mercury vapor on the propagation of the third-harmonic radiation. The quantum-mechanical form of the susceptibility for a single transition frequency can be given as[51]

$$\chi(\omega) = \frac{f\mathrm{Ne}^2/\epsilon_0 \mathrm{mV}}{\omega_0^2 - \omega^2 + \gamma^2 - 2\,\mathrm{i}\omega\gamma} \tag{4.2}$$

where $f = 1.18$ [52] is the oscillator strength of the $6s \longrightarrow 6p$ transition, $\gamma = 0.38\times10^9\ \mathrm{s}^{-1}$ [52] is the natural linewidth, ω_0 is the transition frequency, and N/V is the number density of the mercury vapor in m^{-3}. When the dye laser is tuned to 554nm, the refractive index n_1 and the absorption coefficient α for the third harmonic radiation in mercury are:

$$n_1 \approx 1 + 0.5\times10^{-26}\ \mathrm{N/V} \tag{4.3}$$

and

$$\alpha \approx 3.5\times10^{-24}\ \mathrm{N/V} \quad (\text{ in } \mathrm{m}^{-1}\ ). \tag{4.4}$$

The absorption coefficient α is quite small for the vapor density used, so that the depletion of the third-harmonic is not important, and we observed third-harmonic radiation generated in mercury under this condition. However care should be given to the variation of the refractive index due to temperature changes. A 0.5 °C temperature change in the cold finger will cause a density change of mercury vapor sufficient for a $\pi/10$ shift in the relative phase of the two fields. The intensity of the third-harmonic generated at wavelengths to the red side of the transition is reduced due to phase matching conditions, limiting the study of the interference effect to one side of the transition.

The observation of the interference between the linear and nonlinear transition moments was carried out in the interaction cell. The mercury vapor density in this cell was kept much lower than that in the generation cell. As long as the sensitivity of the multi-photon ionization detection system allows, we would like to keep the mercury density in this cell as low as possible to ensure that the third-harmonic radiation is generated predominantly in the generation cell, and not in this region where the interference is being observed. Maintaining the density of mercury in this cell below 10^{20} m^{-3} assures that the wave vector mismatch in this cell is sufficiently small that the coherence length of the two fields is greater than 16 cm at a laser detuning of 1 nm from resonance. The absorption length of the third-harmonic radiation is calculated to be much greater than the length of this cell for detuning of 1 nm, so that depletion of this field is not a concern.

All the three cells are vacuum sealed and the vacuum system and the argon gas distribution device are shown as in Figure 4.4. The generation cell

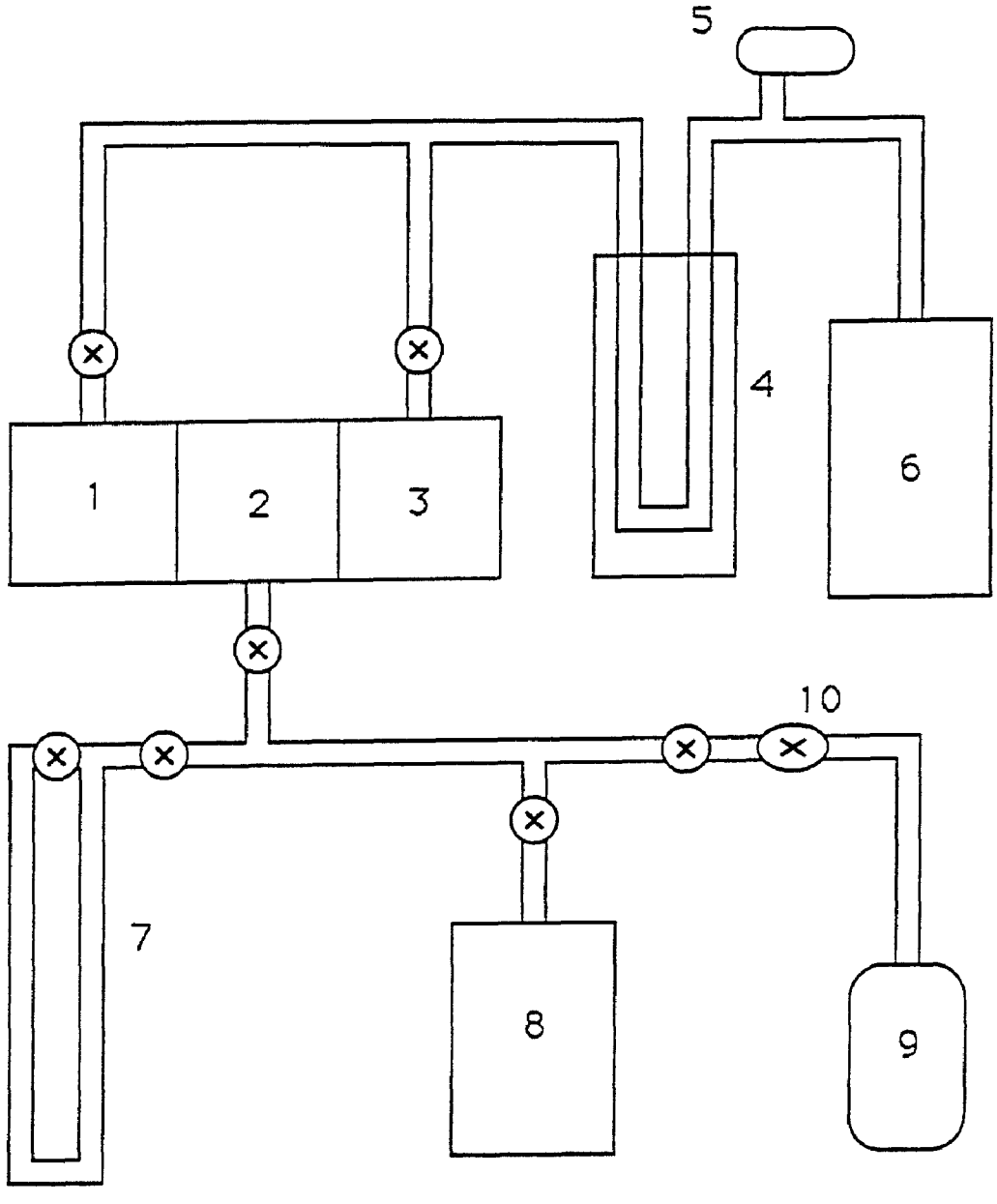

Figure 4.4. Diagram of vacuum system and argon gas distribution device: (1) generation cell, (2) dispersion cell, (3) interaction cell, (4) cold trap, (5) ionization vacuum gauge, (6) diffusion pump, (7) barometer, (8) mechanical pump, (9) argon tank and (10) metering valve.

and the interaction cell are pumped by a Varian HS-2 water cooled diffusion pump with a maximum throughput of 0.5torr liter/second. The backing pump used for the diffusion pump is an Alcatel 2008A mechanical pump, which is not shown in Figure 4.4, with a free air displacement of 7cfm. To avoid mercury vapor getting out of the system a liquid nitrogen cold trap made by a piece of U shaped fused silica tubing and a Dewar bottle is used at times. The cold fingers are wrapped by four to five turns 1/8 inch copper tubings. We run water through the tubing to cool the cold fingers when the vacuum valves attached to the cells are open for long term pumping. When we need to heat the cold fingers to do experiments, we just shut off the running water. The water which remains inside the tubing may improve temperature stability a bit by increasing the thermal mass of the cold fingers. The liquid nitrogen cold trap also helps to reduce the diffusion pump oil back-stream. The pressure of the vacuum system for the two mercury cells is monitored by a Varian 843 rationatic ionization gauge controller and a Varian 571 ionization gauge tube. The maximum vacuum read from the gauge controller was 3×10^{-7} torr. Since the gauge tube is not close to the cells, the maximum vacuum inside the cells would not be as good as the reading and is estimated to be about 10^{-6} torr. During the experiments, the cells have to be closed to provide a constant mercury vapor density. The experiment requires cells which hold a good static vacuum, for several hours without pumping, better than the mercury vapor pressure used for the experiments. With the cells closed, any small leak or outgasing will play a great role in lowering the quality of the vacuum. Strictly speaking, the technique of o-ring seal we used for windows is not good enough for static vacuum. But we have no other alternatives available or affordable. We did everything we could to improve

the static vacuum. The cells have been leak checked many times by two different types of helium leak detector, any suspicious part found has been rewelded, the surfaces of o-ring grooves have been polished, and the o-rings have bee changed time by time. Each time after the cells were open to air for service, the cells were pumped for days, with cell bodies being heated and cold fingers cooled, to get rid of outgasing. We have no direct means to measure the static vacuum. We check it by shutting off the cells for overnight and observing the change of the pressure of the vacuum system when the valve is suddenly opened. By rough estimation, we believe that the vacuum remains better than 10^{-3} torr in 2 hours. This level is deemed acceptable by comparing with the typical mercury vapor pressure used in the generation cell ($\sim$ 0.1 torr) and in the interaction cell ($\sim 3\times10^{-3}$ torr). Here we are in difficulties. On the one hand the stability of the system is important for the experiments such that whenever we change a parameter of experiment we would like to wait until the system is stablized. On the other hand the overall time of data taking is limited to about 2 hours by the mercury cells. As we will discuss later, there is another factor due to the dye laser system which limits the overall data taking time. Hence thorough preparation before the experiment, and careful time management during the data taking are absolutely essential. Usually we prepare the cells for data taking in the following procedure. We heat the cell bodies and pump the cells for at least three hours, with the cold fingers water cooled in this period. When the temperatures of the cell bodies are stablized and the vacuum restored, we shut off the running water for the cold finger and close the cells to start heating the cold fingers. It takes about two hours before the cold finger temperature is stablized. Then we open the cells to pump them again. This time the

pumping can not last too long because the cold finger is now at a higher temperature and more mercury vapor will get out of the system. After about half an hour pumping, we shut off the vacuum valve. Another twenty minutes later the cells are ready for experiment. It seems that twenty minutes is enough for the mercury vapor to get its equilibrium. We have only two hours that the cells can hold the vacuum acceptable for the experiment and we could not afford more time to wait.

The dispersion cell is pumped by a mechanical pump which is shown, with the argon gas distribution system, in Figure 4.4. The argon pressure is measured by a barometer filled with Dow Corning 704 silicone vacuum pump fluid with specific density 1.07 g/cm^3. The accuracy in reading the difference of fluid heights is $\pm$ 1 mm, which corresponds to $\pm$ 0.08 torr accuracy in argon pressure measurement. Before experiments, we pumped the dispersion cell, the barometer and the gas distribution lines; then closed the valve to the vacuum pump and filled the cell with argon to about 50 torr, the maximum pressure that can be measured by the barometer. When the argon pressure needed to be altered to change the relative phase of the two fields, we slowly opened the valve to the vacuum pump to reduce the pressure. The system seems to be disturbed less by scanning argon gas pressure from high to low. The pressure difference between the dispersion cell and vacuum is smaller than that between the cell and the argon source, so that the gas flow is gentler; and we do not introduce any new cold gas into the system during pressure scanning.

The generation cell and the interaction cell are solidly mounted onto the dispersion cell, which is made much stronger mechanically. Then the three

cells, as a rigid body, are bolted down onto the optical table. We hope this will avoid any excessive vibration.

4.3 Dye Laser System

The laser system for this experiment (see Figure 4.5) consists of a tunable pulsed dye laser longitudinally pumped by the frequency-doubled output of a Nd:YAG laser. The YAG laser we have used is a Laserphotonics MY series. Its maximum output at 1.06 μm is 1 J/pulse with a pulse duration of 15ns, and the maximum output of second-harmonic (532nm) was measured to be more than 300 mJ/pulse, with a pulse duration of less than 15ns. The pulse to pulse output energy stability (90% of pulses) at 532nm is $\pm$ 4%. The laser output stability is quite important in nonlinear optics experiments.

The pulsed dye laser is homemade and similar to that described by M. G. Littman[53]. The short cavity length of about 5cm may limit the laser oscillation to a single longitudinal mode under a low pumping level. The pulsed dye laser with a short cavity length supports multiple cavity round trips during the time that the laser medium is active. The gain per pass can be maintained at a relatively low level. Here only a small amount of spontaneous emission is repeatedly and resonantly fed back into the active medium by the cavity. Thus the ratio of the amplified spontaneous emission, which is due to the single-pass amplification with a low gain, to the laser output, which is due to multiple-pass amplification, is quite small. While the low amplified spontaneous emission background is desirable with regard to laser performance, it does make the alignment of the laser more difficult. Another

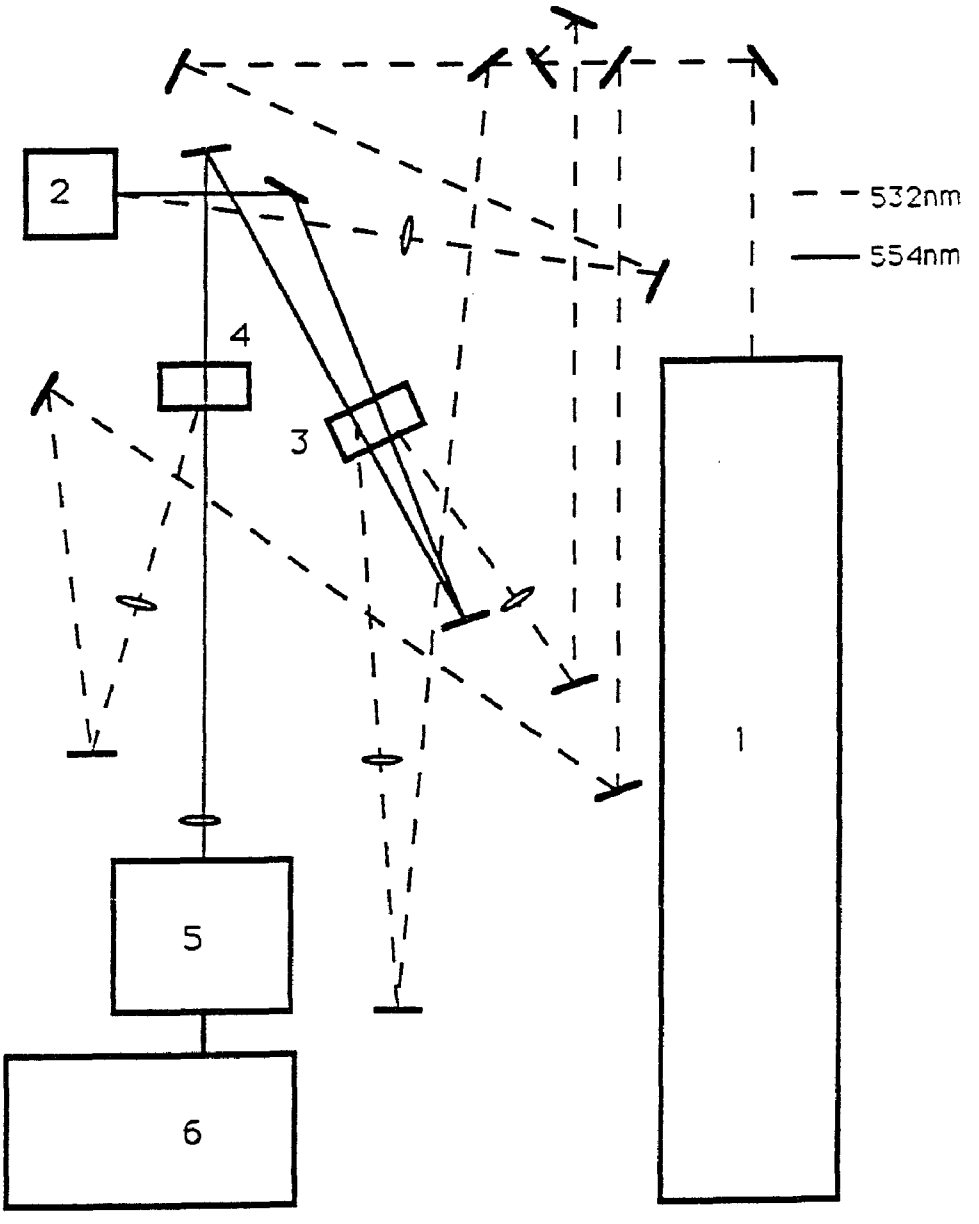

Figure 4.5. Diagram of experimental setup: (1) YAG laser, (2) dye laser, (3) and (4) dye amplifiers, (5) experimental cells, and (6) detection system.

desirable aspect of this laser is that the spatial mode is nearer to TEM_{00} and is more repeatable from shot to shot than conventional pulsed dye lasers. By using 10^{-4} M concentration rhodamine 6G in methanol, we obtain a tunable output range from 552nm to 563nm, with the peak at 560nm and the output at 554nm down to the half.

The output of the dye laser is amplified by two or three stages of dye amplifiers which are longitudinally pumped by the same YAG laser at a time delayed to match the timing of the dye laser beam being amplified. This matching is not only important for increasing the efficiency of amplification but also helpful in reducing the amplified spontaneous emission background. These dye amplifiers are also homemade. In order to ensure the linearity of the polarization of the dye laser beam as well as to increase the efficiency of the dye amplification, the polarization of the output of the dye laser is rotated by a wave-plate before it enters the amplifier, the amplifiers are placed at Brewster's angle, and a high quality polarizer is inserted in front of the first stage of the amplifier. The output energy of the dye laser beam after being amplified can easily reach 20 mJ/pulse at 560 nm and 17 mJ/pulse at 554nm. So far the laser energy needed for our experiments are around several mJ/pulse. We have not yet determined the full energy capability of the laser. The amplified spontaneous emission background as observed by blocking the rear mirror of the dye laser oscillator is very small and can safely be disregarded.

The single-transverse-mode, $TEM_{0,0}$, operation of the dye laser is very crucial in this interference experiment. Since the dye laser system is longitudinally pumped by the second-harmonic of the YAG laser, the

transverse mode of the dye laser is related to the mode structure of the YAG pumping beam. The YAG laser is an unstable cavity and its output is not a well defined Gaussian mode. However the YAG cavity has to be adjusted such that its second-harmonic output is somewhat close to a round and uniform pattern. When adjusting the dye laser oscillator, we insert a prism into its output to reflect it onto a far away white card. By carefully adjusting the mirrors and the position of the YAG second-harmonic pumping beam, we make the dye laser beam profile on the card as round and uniform as possible. Human eyes are easy to get saturated, thus we check the beam profile under different pumping levels. The amplifier stages will affect the beam quality as well. The pumping beams are focused to a proper size to ensure an efficient amplification. The quality of dye laser beam profile is very sensitive to the relative position of the pumping beam and the laser beam at the amplifiers. After all these careful adjustments, the output of the dye laser system is measured to be very close to $TEM_{0,0}$ mode and its beam profile is shown as in Fig. 4.6 and Fig. 4.7. The stability of the dye laser system, which maintains the transverse mode, also sets a limit to the time for data taking. The possible drift of any optical mount or the output position of the YAG second-harmonic will change the dye laser beam structure and ruin the experiment. The time that the amplified dye laser output remains in $TEM_{0,0}$ mode is not predictable and varies from less than an hour to several hours. We could finish our data taking when we were lucky that the dye laser beam structure did not change too much during that time.

As we can see from Fig. 4.6 and 4.7, the beam spot of our dye laser output is elliptical, with a longer spot size in horizontal direction. The beam will have different confocal parameters for its horizontal and vertical behavior.

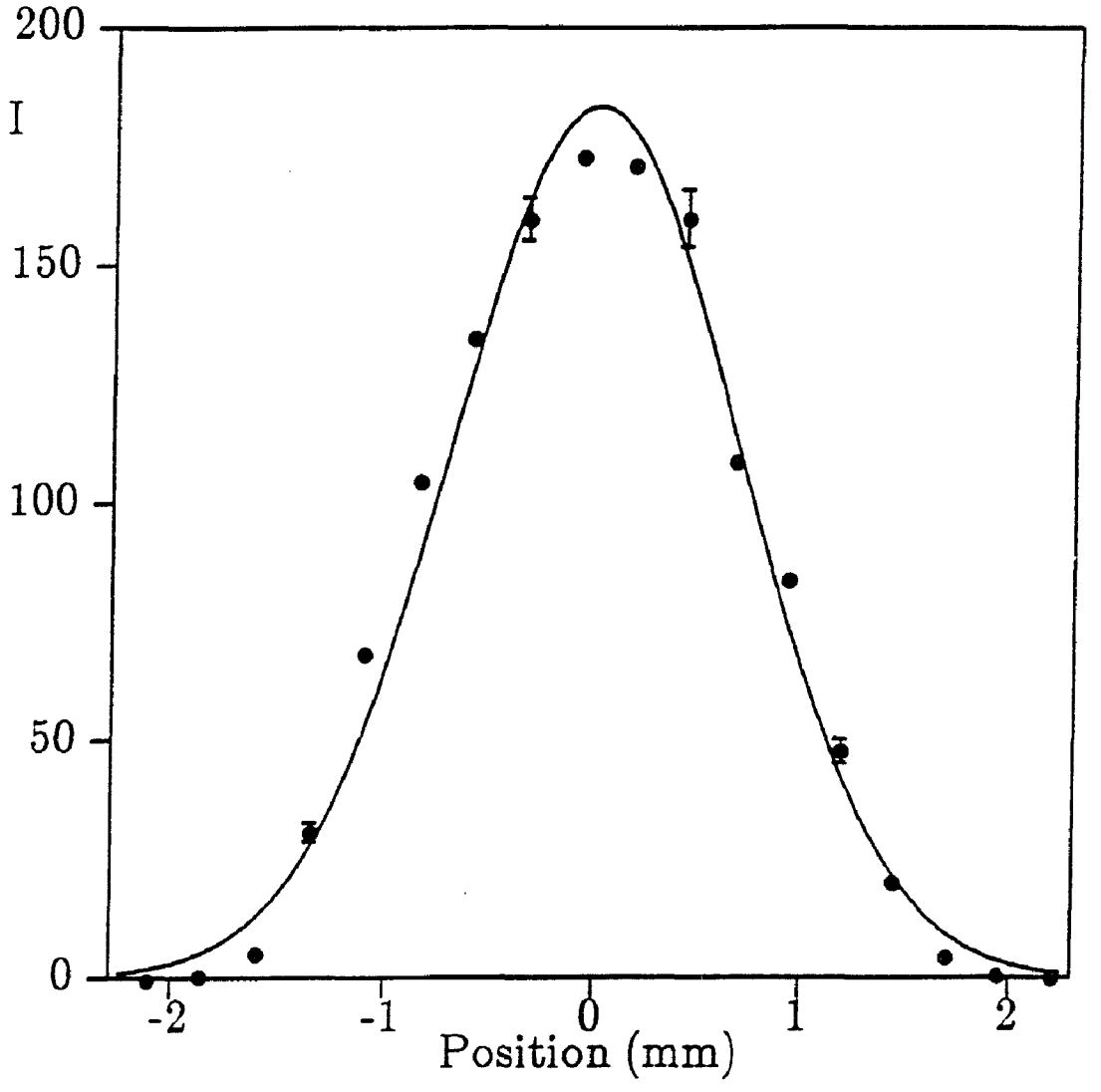

Figure 4.6. Beam profile of the dye laser output measured along the horizontal axis. Error bar shows standard deviation of the mean. Solid line indicates a best fit to the data.

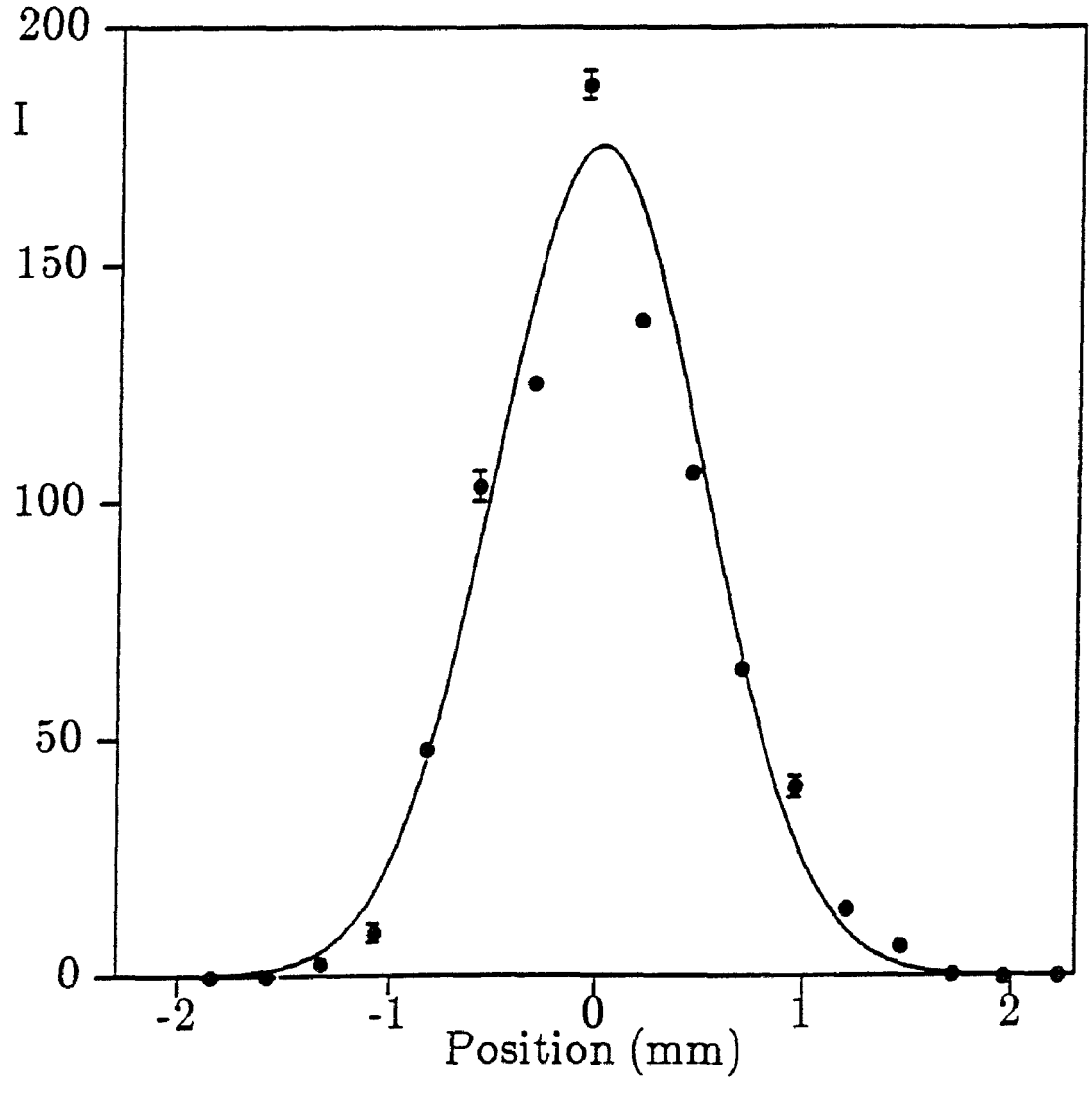

Figure 4.7. Beam profile of the dye laser output measured along the vertical axis. Error bar shows standard deviation of the mean. Solid line indicates a best fit to the data.

This makes the mathematical expressions more complicated but not the physics. We will not go into this mathematical complexity except for Section 5.3 in the next chapter, where the confocal parameters are explicit parameters in the final expression.

The amplified dye laser beam is focused by a lens into the experimental cells. The beam waist radii w_{0x} and w_{0y} at focus are estimated as 25 μm and 35 μm, and the peak power density corresponded is about 20 GW/cm^2 when a laser output of 5 mJ/pulse and a 20 cm focal length lens are used.

4.4 Detection and Data Treatment

The multiphoton ionization signals from the interaction cell are simply collected with the electrodes biased by a positive voltage chosen from +9 to +300V. Then the signal is AC coupled into a preamplifier. When the multiphoton ionization signal is relatively small or the electrodes are biased by a lower voltage, a high gain amplifier, LeCroy TRA402, is used. It has a gain of 25 mV/μA, a rise-time less than 3 ns and a low input noise less than 65 nA rms. When the signal is strong or the electrodes are biased by a higher voltage, a faster amplifier, LeCroy VV100B, is used. It has a fixed and stable gain of 10, a rise-time less than 2 ns and a linear-response input range of -0.5V (or to +0.01 V for positive pulses). The choice of bias and amplifier are determined by the experiment conditions. The higher voltage bias definitely will give a sharper and clearer signal but modifies the experiment condition as well. This will be discussed later.

Detection of the third-harmonic radiation is not so easy as that of the multiphoton ionization signal. The third-harmonic radiation has to be

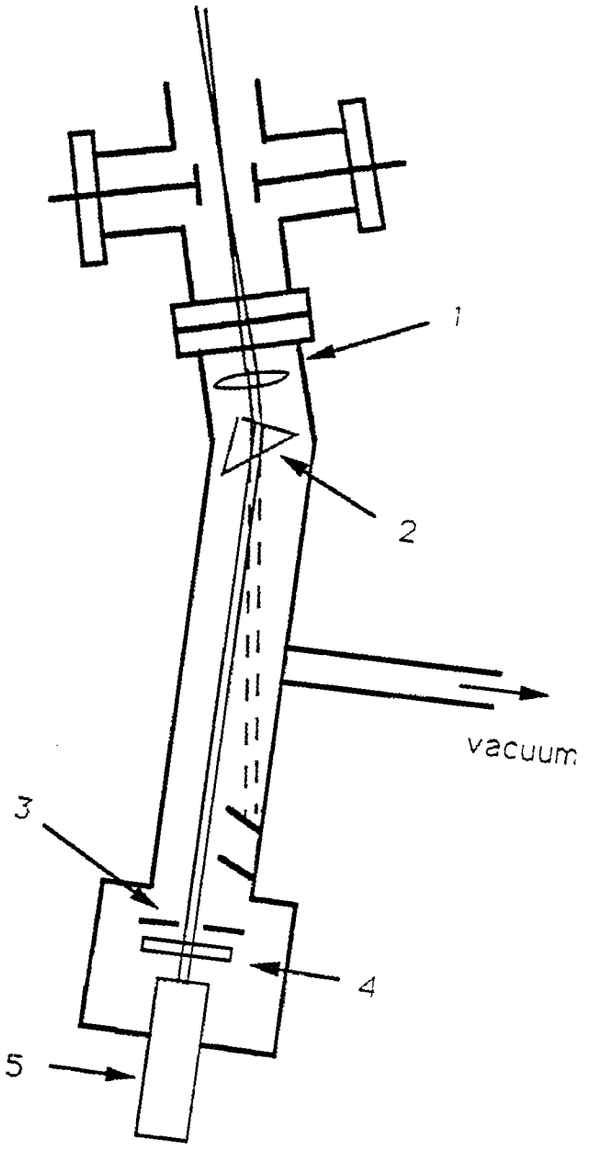

Figure 4.8. Diagram of the third-harmonic detector: (1) 7.5 cm lens, (2) prism, (3) aperture, (4) UV filter, and (5) solar blind photomultiplier.

separated from the intense fundamental beam. Moreover it must be kept in a vacuum environment to avoid being attenuated through absorption by the air. The third-harmonic detector is shown in Figure 4.8. The beams are collimated by a UV grade 7.5cm lens and separated by a UV grade prism. The laser line filter used is Acton 183-B-1D, with peak transmittance 33.8% at 181nm and bandwidth 42 nm. Finally, the third-harmonic signal is detected by a solar-blind photomultiplier, Hamamatsu R1893, which has a spectral range from 162 nm to 320 nm, a 0.8ns rise-time and an anode radiant sensitivity of 3 A/mW. The fundamental laser beam is so intense that the background of 554nm still exists after all these efforts.

The intensity of the dye laser output is monitored by a photodiode, EG&G SGD040 (rise-time 3 ns, responsivity 0.26 A/W at 555 nm). All these signals being detected, including 1) the preamplified multiphoton ionization signal, 2) the third-harmonic generation signal and 3) the dye laser intensity signal, are sent to a computer controlled data system. The signals are integrated and converted into digitized data by a gated analog-digital converter, LeCroy Model 2249SG. A discriminator, LeCroy Model 821, which is triggered by a photodiode signal or by the synchronization signal from the YAG Q-switch, provides the 50ns wide gate signal to control the analog-digital converter. Only data in those shots for which the dye laser intensity falls within a $\pm$ 5% window are accepted to be averaged, the others are discarded. Delay cables are used to match the correct timing for the gate and the signals and the timing are checked on a Tektronix 11302 500MHz oscilloscope with high-writing-rate microchannel-plate CRT display bright enough to view fast pulse transients in normal room light.

Since the Q-switched YAG laser is a strong electrical noise source and the signals to be detected are relatively weak, great effort has been made in grounding and shielding to increase the signal-to-noise ratio. The preamplifier is directly connected to the electrical feedthrough on the interaction cell. The voltages supplied to the preamplifier are filtered and their values are optimized to give a better signal-to-noise ratio. The amplified multiphoton ionization signal is sent to the analog-digital converter through double shielded coaxial cable. After all these efforts, the typical signal level reaches 200mV to 400mV with a noise level of around 30mV. This will be further improved by integration of the analog-digital converter and data averaging since the probability of the noise going positive or negative should be equal.

CHAPTER 5

EXPERIMENTS AND RESULTS

5.1 Single-Cell Experiment

As a preparation for the interference experiment reported here, a single-cell experiment was carried out by using only the interaction cell and removing the other two cells. The results are in a good agreement with those reported by D. Normand, *et al*[10], and shown in Figure 5.1 and Figure 5.2. It is easy to see from those figures that the multiphoton ionization and third harmonic generation related to the 6s-6p transition are peaked at 554nm. We accordingly used this wavelength in the interference experiments which are reported in the next two sections. The dye laser output used in this single-cell experiment was 2 mJ/pulse and a 11 cm lens was used to focus it into the mercury cell. The wavelength was calibrated by a monochromator, PTI 01-001. The reading from the micrometer of the the home made dye laser and the wavelength measured by the monochromator have a very linear relation and this makes the wavelength calibration and conversion quite easy. The efficiency of the dye laser system varies at different wavelengths. Thus some adjustment of the YAG laser output intensity was required during the wavelength scanning to keep the dye laser pulse energy nearly constant such that a larger portion of the laser shots fell into the intensity limit window set by the computerized data acquisition system. Each time the cell was pumped before experiment and then shut off to avoid effects from impurities and

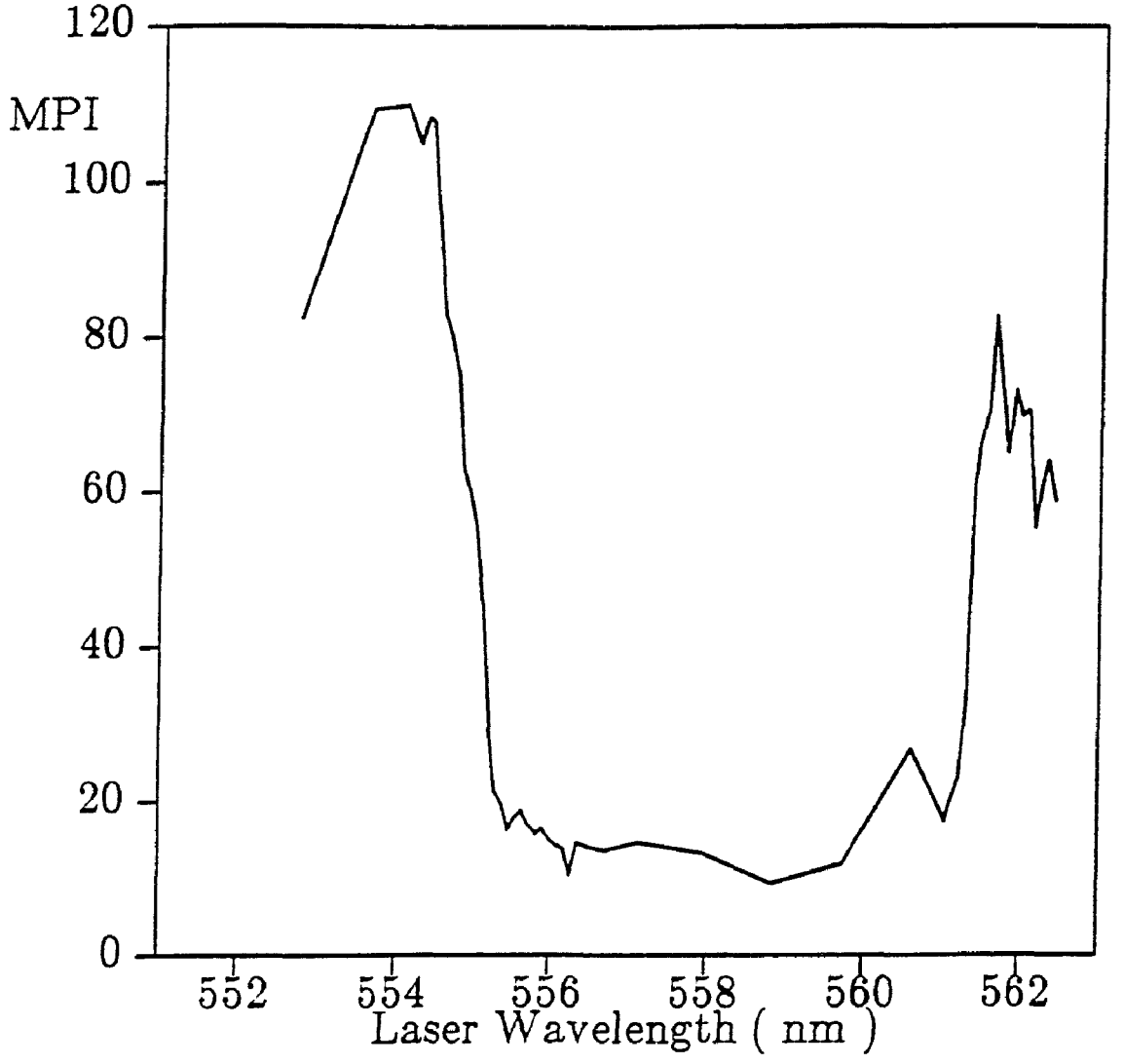

Figure 5.1. The multiphoton ionization signal as a function of laser input wavelength.

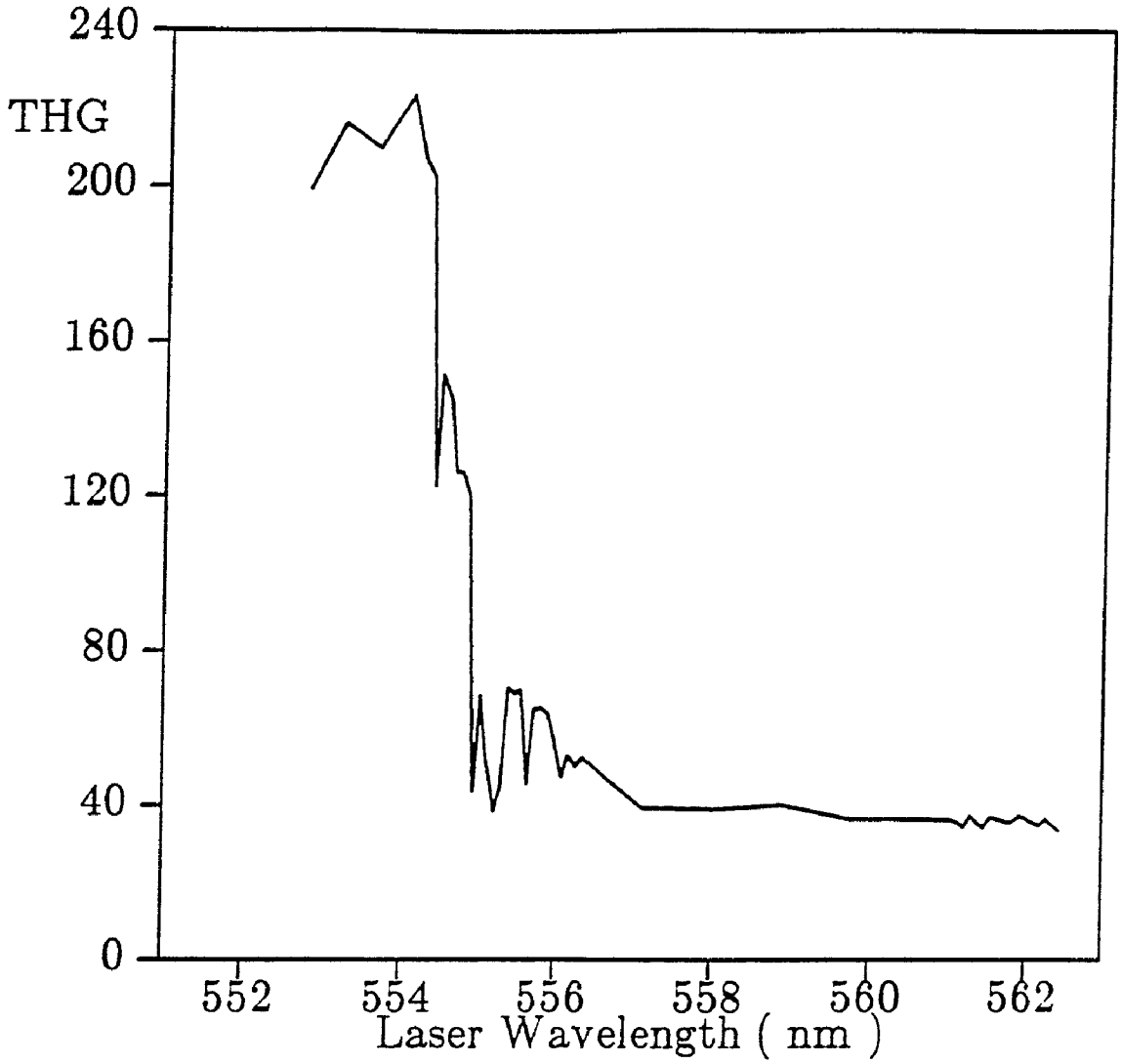

Figure 5.2. The third-harmonic generation signal as a function of laser input wavelength.

pollution of the mercury. During the experiments the body of mercury cell was constantly kept at a temperature above 80°C except for the cold finger. The density of the mercury vapor, determined by the temperature of the cold finger (the coldest spot in the closed cell), was controlled to be a desired value. A very interesting thing was that when we used 300 V bias to observe the dependence of the multiphoton ionization signal on the density of the mercury vapor, the multi-photon ionization signal kept growing up as the temperature of the cold finger increased to 80°C. While using +9 V bias, the results were different and were shown in Figure 5.3. The multiphoton ionization signal started to drop after the temperature got 50°C, due to the "competition" between third-harmonic generation and multi-photon ionization. We believe there exists the secondary ionization caused by accelerated electrons under 300 V bias. The secondary ionization amplifies the signal and its gain depends on the mercury density. When the mercury vapor density increases as the temperature of the cold finger gets higher, the laser induced multi-photon ionization decreases but the chances that the signal gets amplified by secondary ionization increase, preventing the observed signal from dropping with temperature increasing as we expected. We also believe this secondary ionization amplification at higher bias could be helpful in some cases as long as the vapor density in the mercury cell does not change much during data taking.

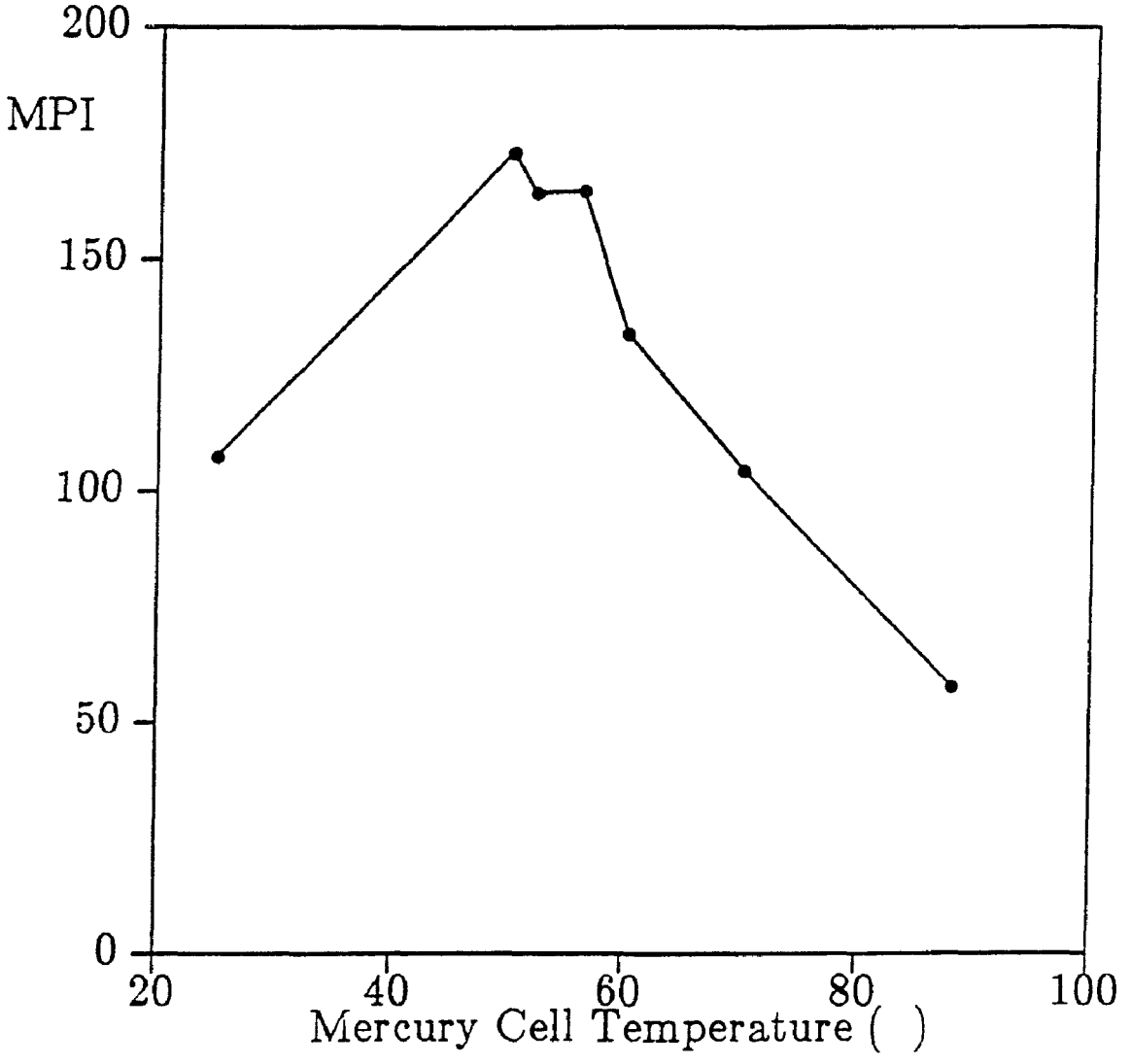

Figure 5.3. Dependence of the multiphoton ionization signal on the temperature of the cold finger of the mercury cell.

5.2 Experiment of Interference between Transition Amplitudes by Monitoring the Total Ionization Rate

In this experiment[54], we studied the interference between one-photon and three-photon 6s-6p transitions in mercury by observing the dependence of the multi-photon ionization on the relative phase of the two fields. We used all three cells as described in Chapter 4 (see Figure 4.1). The 554nm dye laser output was focused by a 20cm lens into the generation cell to generate third-harmonic radiation at about 185nm. Then the two fields diverged into the dispersion cell where they were refocused by the mirrors into the interaction cell. The phase of the two fields were delayed by a different amount by the argon gas in the dispersion cell providing the means to control the relative phase of the two fields. In the interaction cell the two fields excited the mercury atoms by one-photon transition and three-photon transition respectively. The atoms were further ionized by absorbing two additional photons from the fundamental field. The ionization signal, as a measure of the net transition moment, was monitored by collecting all the electrons ionized by the optical fields in the entire interaction region with a pair of plate electrodes, one is grounded to the cell body and the other is biased +24V.

As we can see from the structure of the experimental cells, the two mirrors in the dispersion cell form a 1:1 optical imaging system. The beam waist of the dye laser output at the focus in the interaction cell is approximately the same as that in the generation cell. Both of them are determined by the focal length of the lens we used to focus the dye laser beam into the generation cell. In this interference experiment, the overlap of the two beams is very important. It will be easier to achieve transverse overlap if a

lens of a longer focal length is used since the beam size of the two fields at focus is larger under a loose focusing. But the focal length can not be too long either. If the focal length is very long, the divergence angle of the fields will be small and the beam spot size at the mirrors, which are 25 cm away from the focuses and at the windows, which are roughly 5 cm away from the focuses in the generation cell as well as in the interaction cell, will be smaller, comparing with the case of tight focusing. Moreover, a higher intensity of the dye laser output is required to maintain the same power density to induce the nonlinear optical interaction because of the larger beam size at the focus. Thus the power density of the dye laser beam at the mirrors and the windows will be much higher when a lens of a longer focal length is used and it will definitely cause damage to the mirrors and may cause damage to the windows especially when the windows are not perfectly clean. We tried different lenses and found that a lens with a 20 cm focal length served better. In this case, the confocal parameter ($2z_0$) of the two fields, which is approximately the length of the interaction region, is close to 1 cm, the dimension of the collecting electrodes. This may help to collect the ionized electrons more effectively. In the single-cell experiment where a 11 cm lens was used, the output of the dye laser used was 2 mJ/pulse. While a 20 cm lens is used in this experiment, a higher intensity of 4.5 mJ/pulse is required to provide a signal several times larger than the noise background. This power level is still quite high with regard to the damage threshold of the the aluminum coating on the two mirrors. We burned many spots on the coatings during the experiment. Each time the mirror burned, we had to rotate it to use another part of its surface. After we finished the experiments, there are so many burned spots on the mirrors that they are not useful any more. Recently we

bought another pair of mirrors with a longer focal length and modified the dispersion cell accordingly. The new mirrors no longer get burned.

The total ionization signal is expected to be given by integrating the ionization rate over the entire region. But we can not directly integrate Equation 3.19 because the integration of Equation 3.19 over entire space does not converge. Equation 3.19 requires that the ionization step be saturated. To give some ideas about the total ionization signal and the possible modulation depth of the interference, we consider the unsaturated case by weighting Equation 3.19 with an additional factor of I^2, which is the dependence of the ionization step on the intensity of the fundamental field. The integration converges and gives the total ionization rate as:

$$W_{tot} \propto 1 + \frac{5}{8}M^2 + \frac{M}{2}\cos(3\phi_2 - \phi_1), \tag{5.1}$$

where the phase matching condition of Equation 3.20 has been used and

$$M = \frac{\mu_3 E_2^3}{\mu_1 E_1} \tag{5.2}$$

represents the ratio of the contributions of the two processes at the beam waist on axis. When M=1, the two transition amplitudes are matched at z=0, where the beam waists locate, and the single-photon transition amplitude will be larger at any other places. When M=2, the two transition amplitudes are matched at $z=\pm z_0$. The single-photon transition amplitude will be larger for $|z| > z_0$ and smaller for $|z| < z_0$. The depth of modulation, defined as the ratio of the amplitude of the sinusoidal component and the average ionization rate, (the ratio of M/2 and $1 + M^2$ in this case), has a maximum value of $\sqrt{0.1}$ (about 30%) at $M=\sqrt{1.6}$. Since focused beams are

used, the transition amplitudes can be matched at no more than two places. The positions of amplitude matching are determined by the transition amplitude ratio M, but the depth of modulation of the total ionization rate does not depend strongly on the ratio M because of the averaging effect of the integration, and is within 10% of the maximum value from M=3/4 to M=2. The results of multi-electrodes experiment will show in the next section that the ionization step, under our experimental conditions, seems saturated in the focal region. Generally speaking, the depth of modulation will be less than this maximum value when the ionization step is saturated because the dependence of the ionization on the intensity will be a lower-order and the ionization is no longer confined in the focal region so strictly as it is in the unsaturated case. The dephasing factor of $\tan^{-1}\left(\frac{z}{z_0}\right)$ will play a greater role in reducing the interference signal in total ionization rate. Thus the experimental system is required to be highly stablized and optimized in order to observe the interference signal of a possible depth of modulation less than 30%.

We prepared the cells and adjusted the dye laser system before experiments, following the procedures described in the previous chapter. We carefully planned such that the cells and laser system were ready for taking data at almost same time. It seems that the normal incidence of the fields onto the rear window of the generation cell and the front window of the interaction cell is much more critical than we estimated by calculation. Because the reflected spot from the front window of the interaction cell could not be found outside the cells, we had to align it by opening the dispersion cell. And we could not monitor this normal incidence during the experiment.

It happened to be that we could hardly get any good results whenever we did some major alignment to the dye laser system just before the experiment. Usually, after a day or so the laser system stablized. If only a small adjustment was needed at that time, the chances of obtaining satisfactory results were much higher. The results of this experiment are as shown in Fig. 5.4 Each data point in Fig. 5.4 represents the average value of sixty to eighty laser shots. the error bars indicating typical standard deviation of the mean are shown for a few data points. The solid line is fitted to the data by adjusting the amplitude, period and phase of a cosine function and the average DC value. We can clearly see that the total ionization signal is modulated by changing the argon pressure. The pressure difference of the argon required to change the phase by 2π is approximately 6.1 ± 0.6 torr, which yields a refractive-index difference of $(4.6 \pm 0.4)\times10^{-5}$ of argon for 185nm and 554nm. This is in a reasonable agreement with extrapolations of refractive-index data reported previously for argon,[46] $\Delta n = 4.5\times10^{-5}$. The depth of modulation shown in the figure is only 15%. Deviation from the calculated maximum possible value of 30% could be due to a number of factors such as incomplete beam overlap, nonoptimal ratio of the transition amplitudes (M), imperfect $TEM_{0,0}$ laser beam, saturation of the ionization step and locally generated third-harmonic generation. Among these factors, we believe, the last two are the main reasons causing the depth of modulation lower than the calculated possible value. In this experiment, the temperature of the cold finger of the interaction cell was set at about 30°C (80°C for the generation cell) and the intensity of the dye laser beam was 4.5 mJ/pulse. We will show in the next section that the saturation of the ionization step and "phase locking" due to locally generated third-harmonic do exist under this

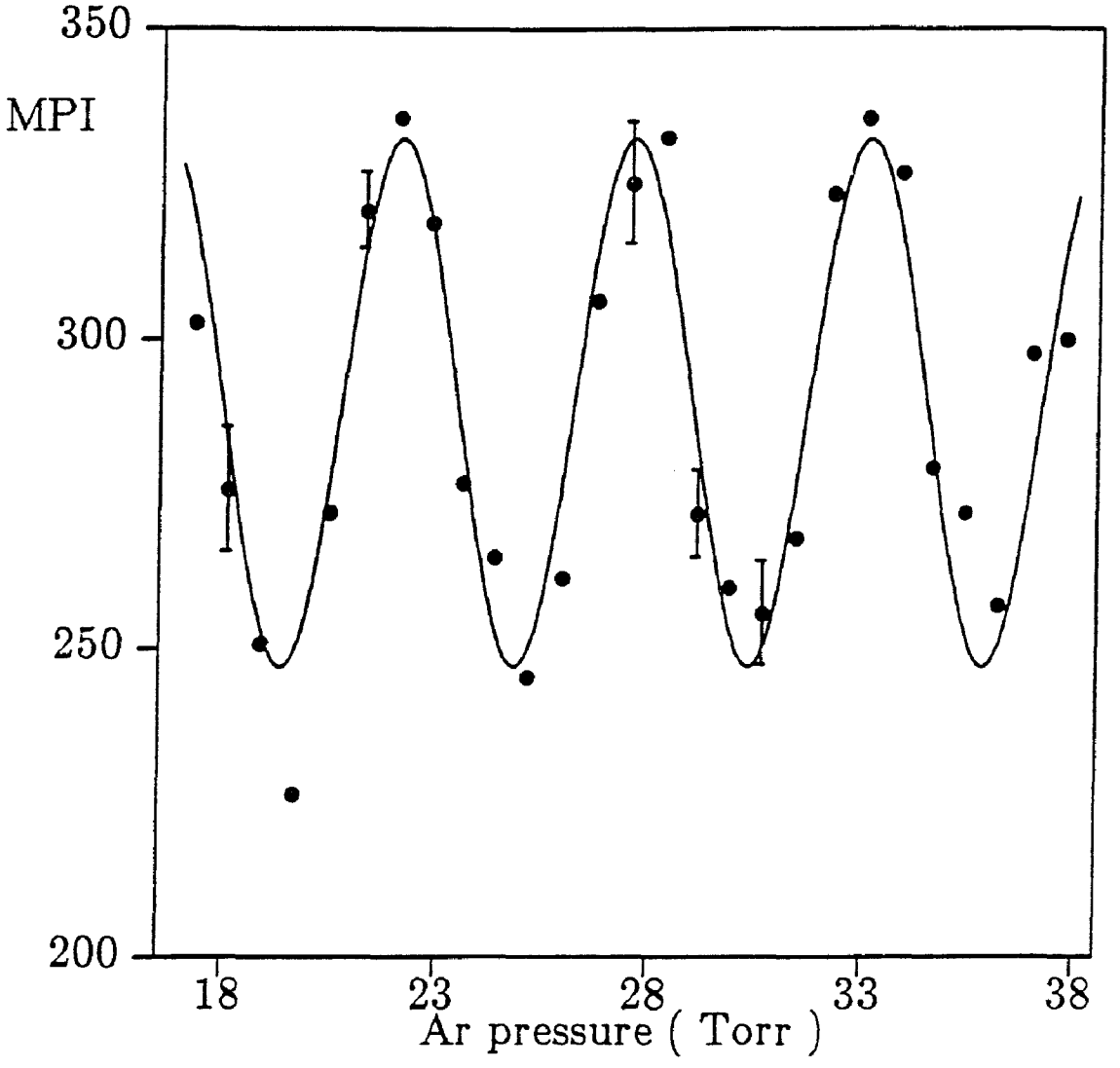

Figure 5.4. Total ionization signal as a function of argon pressure. Typical standard deviation of the mean are shown for a few data points. The solid line represents a best fit for the data.

condition.

5.3 Experiment to Measure Optical Phase Variations Using Interfering Multiphoton Ionization Process

In last section, we discussed the possible maximum value for the depth of modulation of the interference signal, monitored by collecting the photo-ionized electrons from the entire interaction region. Among factors limiting that value, the $\tan^{-1}(\frac{z}{z_0})$ phase term of the Gaussian beam plays a dominant role. But it also makes itself, for the first time, an observable. People have known this phase term for a long time as a necessity for the Gaussian beams to satisfy the wave equations. It has been used in the explanations to the transverse mode spacing in an optical cavity,[55] and the phase matching conditions in harmonic generations by focused laser beams[45]. The opportunity comes to us now to measure directly this phase term. Due to the $\tan^{-1}(\frac{z}{z_0})$ phase term, the relative phase between the one-photon and three-photon transition amplitudes varies along the beam axis and changes interference condition. If we detect the multi-photon ionization signal from sections at different distances from the focus along the beam axis in the interaction cell, separately but simultaneously, we should be able to find the phase variation among these interference signals from different sections.

In this experiment[56], the experimental system and experimental conditions we used and the experimental procedures we followed are very similar as we discussed before except for the collection electrode in the interaction cell, which was redesigned as a set of eight biased collection

electrodes. The schematic diagram of the interaction cell with the set of eight electrodes is shown in Fig. 5.5. Each electrode was constructed from a 1.27 mm diameter stainless steel rod. They are aligned transverse to the direction of the laser beam, side by side with a center-to-center spacing of 1.65 mm, in a plane parallel to and 1 cm above the surface of the grounded electrode. Each electrode is sensitive to the electrons generated in the section directly between it and the grounded plane electrode. The spatial resolution of this detector is limited by the spacing between adjacent electrodes and some signal redistribution among sections due to the trajectory of the free electrons in the collection field. The laser beam propagated between the plane of the eight electrodes and the ground electrode along an axis parallel to those planes. To increase the spatial resolution, the laser beam was aligned closer to the eight electrodes (the laser fields could cause photo-electric effect on the surfaces of the electrodes if the beam is too close to the electrodes), and the eight electrodes were biased to a relatively high voltage, 90 V. The maximum horizontal displacement of the free electrons was calculated, under these conditions, less than the center-to-center spacing of the electrodes. By adjusting the position of the focussing lens in front of the generation cell, the focal region of the laser beam was approximately centered and the detector covered roughly the entire interaction region, from $-z_0$ to $+z_0$. The multi-photon ionization signals collected by the electrodes were sent to a home-made eight-channel preamplifier which was directly connected to the electrodes. Then the amplified signals were integrated, averaged and recorded by the computer controlled data acquisition system, which has been discussed in Chapter 4.

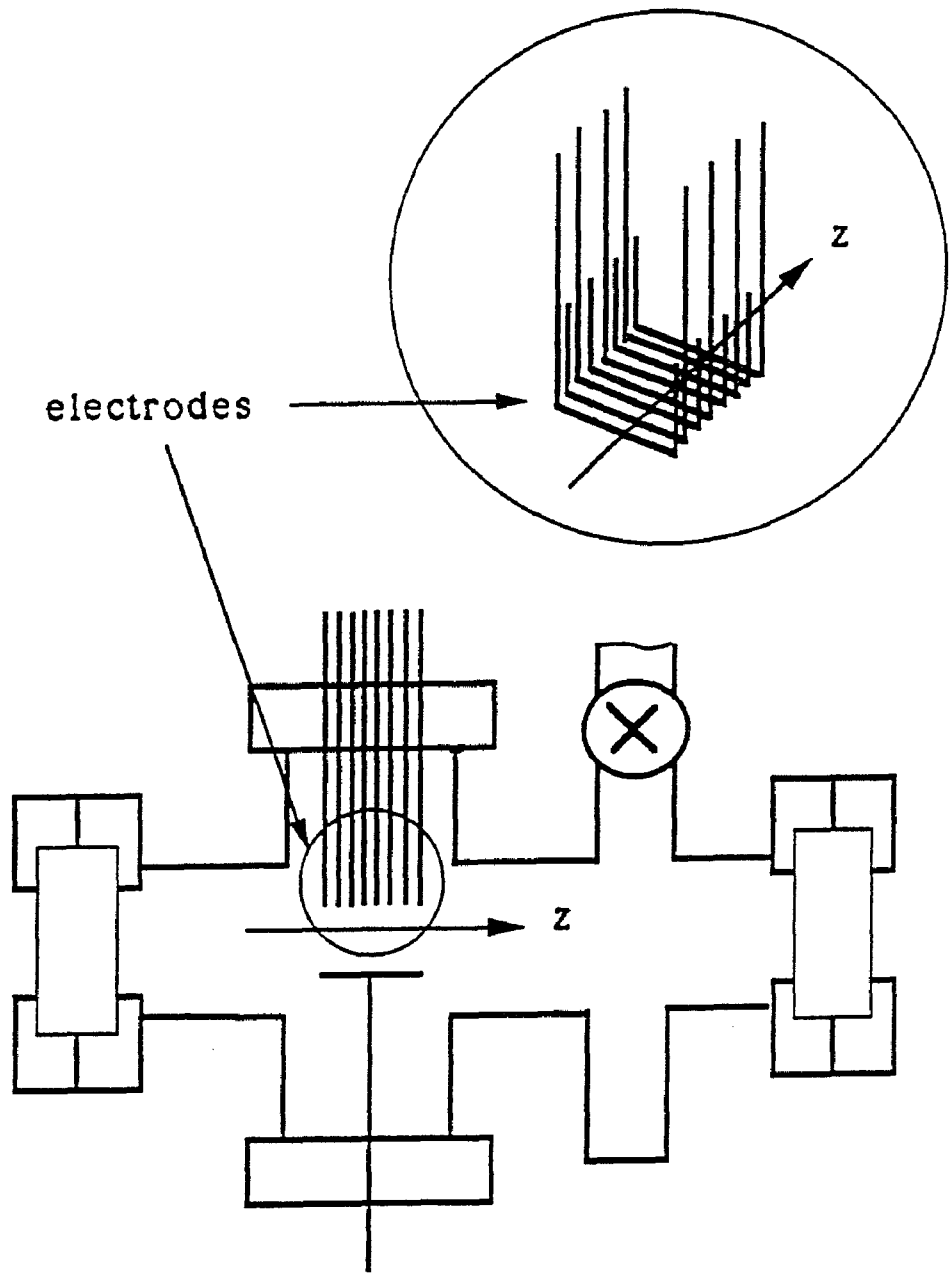

Figure 5.5. Schematic diagram of interaction cell with multi-electrodes.

Since each electrode is sensitive to electrons ionized in a section at a certain distance z from the focus, we need to integrate Equation 3.19 over the transverse dimensions, yielding:

$$W(z) \propto 1 + \frac{M^2}{[1+(\frac{z}{z_0})^2]^2} + \frac{2M}{[1+(\frac{z}{z_0})^2]}\cos(3\phi_2 - \phi_1 + 2\tan^{-1}(\frac{z}{z_0})), \tag{5.3}$$

where the phase matching condition of Equation 3.20 has been used and M, as defined before, represents the ratio of the contributions of the two processes at the beam waist on axis. The confocal parameter z_0 is explicit in Equation 5.3. We would generalize it into an expression for the elliptical Gaussian beams we used in our experiments. The expression for an elliptical $TEM_{0,0}$ Gaussian beam propagating along z axis can be given as:

$$E(x,y,z) = \frac{E}{[1+(\frac{z}{z_{0x}})^2]^{\frac{1}{4}}[1+(\frac{z}{z_{0y}})^2]^{\frac{1}{4}}} \exp\left[-\frac{x^2}{w_x^2(z)} - \frac{y^2}{w_y^2(z)}\right] \times \exp\left\{-i\left[kz - \phi - \frac{1}{2}\tan^{-1}(\frac{z}{z_{0x}}) - \frac{1}{2}\tan^{-1}(\frac{z}{z_{0y}})\right]\right\}, \tag{5.4}$$

where the radial phase factor has been omitted, the factors are defined similarly as those in Equation 3.9 and the subscripts x, y denote the horizontal and vertical axes respectively. The "spot sizes" $w_x(z)$ and $w_y(z)$, defined as the $1/e^2$ intensity beam radius, varies along z axis as:

$$w_i(z) = w_0[1+(\frac{z}{z_{0i}})^2]^{\frac{1}{2}}, \qquad i = x,y, \tag{5.5}$$

where $w_{0i} = w_i(0)$ are the minimum "spot sizes" or beam waists for the elliptical Gaussian beam. The confocal parameters, z_{0x} and z_{0y}, are defined as:

$$z_{0i} = \frac{\pi w_{0i}^2}{\lambda}, \qquad i = x,y. \tag{5.6}$$

They are much the same as those for the circular Gaussian beam. The relations between the laser field and its third harmonic generation we derived in Chapter 3 remain valid and Equation 5.3 can be easily generalized for the elliptical beams as:

$$W(z) \propto 1 + \frac{M^2}{\left[1 + (\frac{z}{z_{0x}})^2\right]\left[1 + (\frac{z}{z_{0y}})^2\right]} + \frac{2M}{\left[1 + (\frac{z}{z_{0x}})^2\right]^{\frac{1}{2}}\left[1 + (\frac{z}{z_{0y}})^2\right]^{\frac{1}{2}}} \times$$

$$\cos(3\phi_2 - \phi_1 + \tan^{-1}(\frac{z}{z_{0x}}) + \tan^{-1}(\frac{z}{z_{0y}})). \tag{5.7}$$

The ionization signals detected by six of the eight electrodes are shown in Figure 5.6 as functions of the argon pressure in the dispersion cell. The first electrode and the last electrode were positioned far from the laser focus such that only a weak ionization signal was collected, resulting in an unsufficient signal-to-noise ratio. Each data point in Figure 5.6 represents the average ionization signal over 60 to 80 laser shots. For each electrode data set, the average DC level of the ionization signal has been subtracted leaving only the part which varies with the argon pressure. Each data set is seen to vary sinusoidally with a period of around 6-7 torr in argon pressure change. A phase shift of the signal from one electrode to the next can be observed in the figure. This phase shift is due to the $\tan^{-1}(\frac{z}{z_0})$ terms in Equation 5.7. By

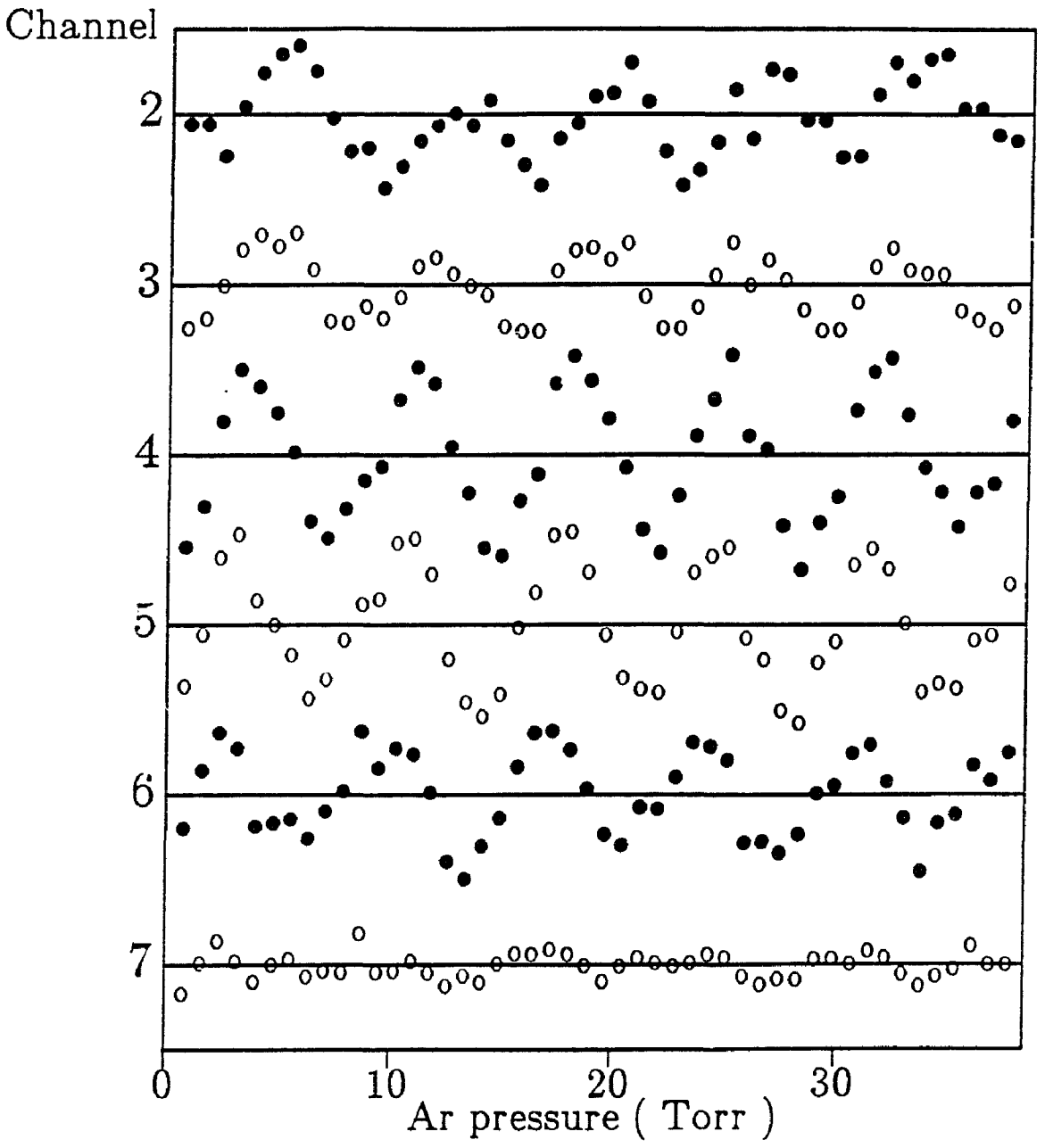

Figure 5.6. Ionization signal as a function of argon pressure for individual electrodes. The average DC level of the ionization signal has been subtracted from each data set.

fitting a sinusoidal curve to each data set, the relative phase shift of the ionization signal of each electrode can be determined. These relative phase shifts are shown in Figure 5.7 and Figure 5.8. The error bars represent the estimated error in the phase, as determined from the standard deviation of the ionization signals. The solid lines represent the compensation for the $\tan^{-1}(\frac{z}{z_{0x}}) + \tan^{-1}(\frac{z}{z_{0y}})$ terms in Equation 5.7. The values of z_{0x} and z_{0y} are derived from the measurements of the beam radii of the nearly Gaussian beam before being focused into the generation cell as shown in Figure 4.6 and 4.7 and the focal length of the lens used in experiment. Figure 5.7 shows data of the experiment in which a 20 cm focal length lens was used, resulting in $z_{0x} = 3.65$ mm and $z_{0y} = 7.05$ mm. Figure 5.8 shows data for a 17 cm focal length lens, corresponding to $z_{0x} = 2.64$ mm and $z_{0y} = 5.10$ mm. The location of the focus ($z = 0$ point) in the figures was determined to within 1 mm from the z dependence of the ionization signal measured directly after each experiment when the third harmonic generation was absent as the generation cell being cooled and evacuated. The only fully adjustable parameter in the figures is, therefore, a vertical offset of the data since these measurements can determine only the relative phase. In both of the figures, the data and calculations are in a good agreement.

Since the intensity of the laser beam varies through the focal region and each of the eight electrodes is sensitive to the electrons ionized in a section at certain distance from the focus, we can measure the intensity dependence of the multi-photon ionization process especially in a noninterfering case. We simply ran cooling water to cool the cold finger of the generation cell and evacuated it to avoid third- harmonic generation in mercury vapor. Only the

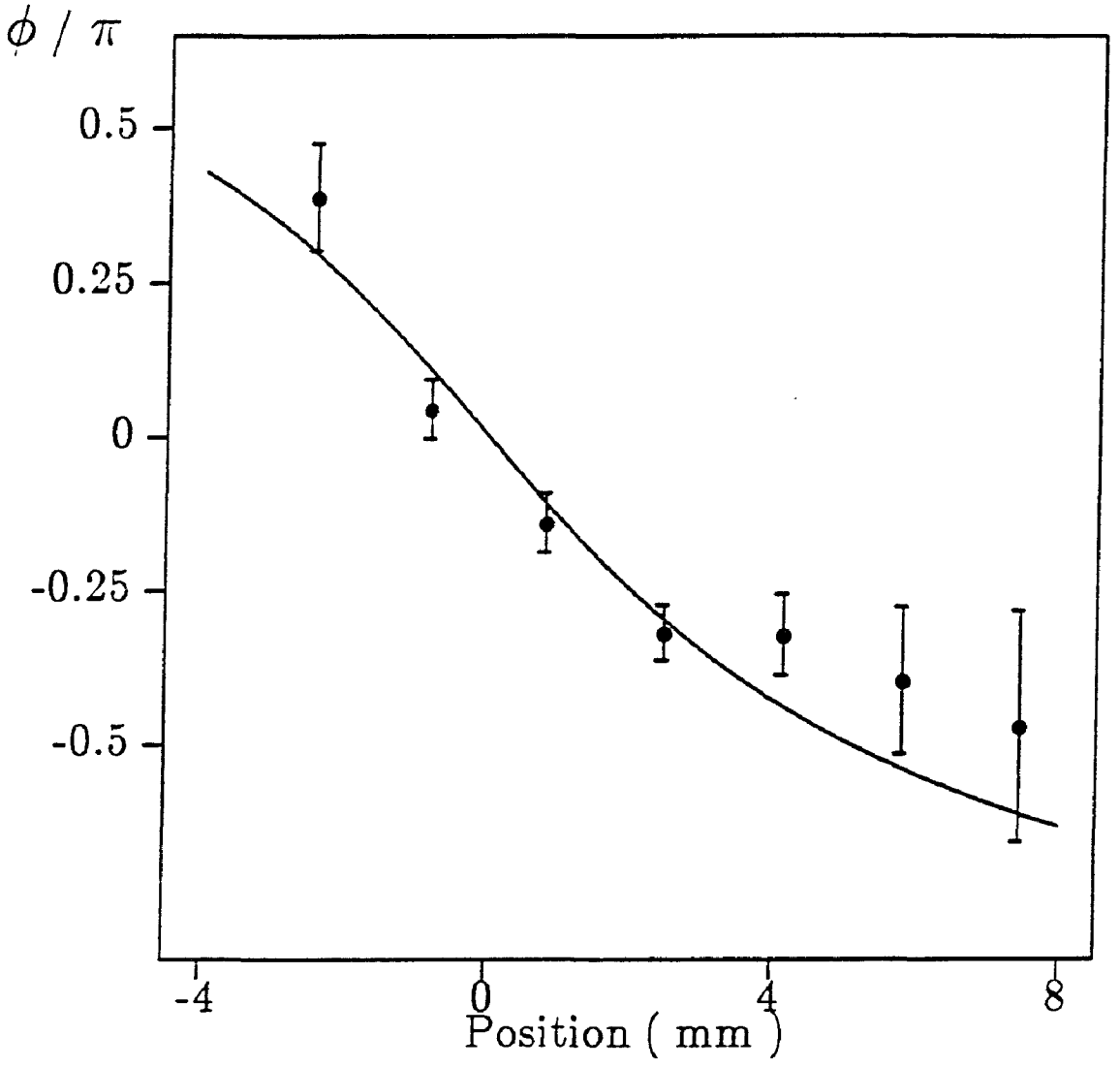

Figure 5.7. The relative phase of the ionization signal as a function of z, the distance from the laser beam focus, for $z_{0x} = 3.65$mm and $z_{0y} = 7.05$mm when a 20 cm lens is used.

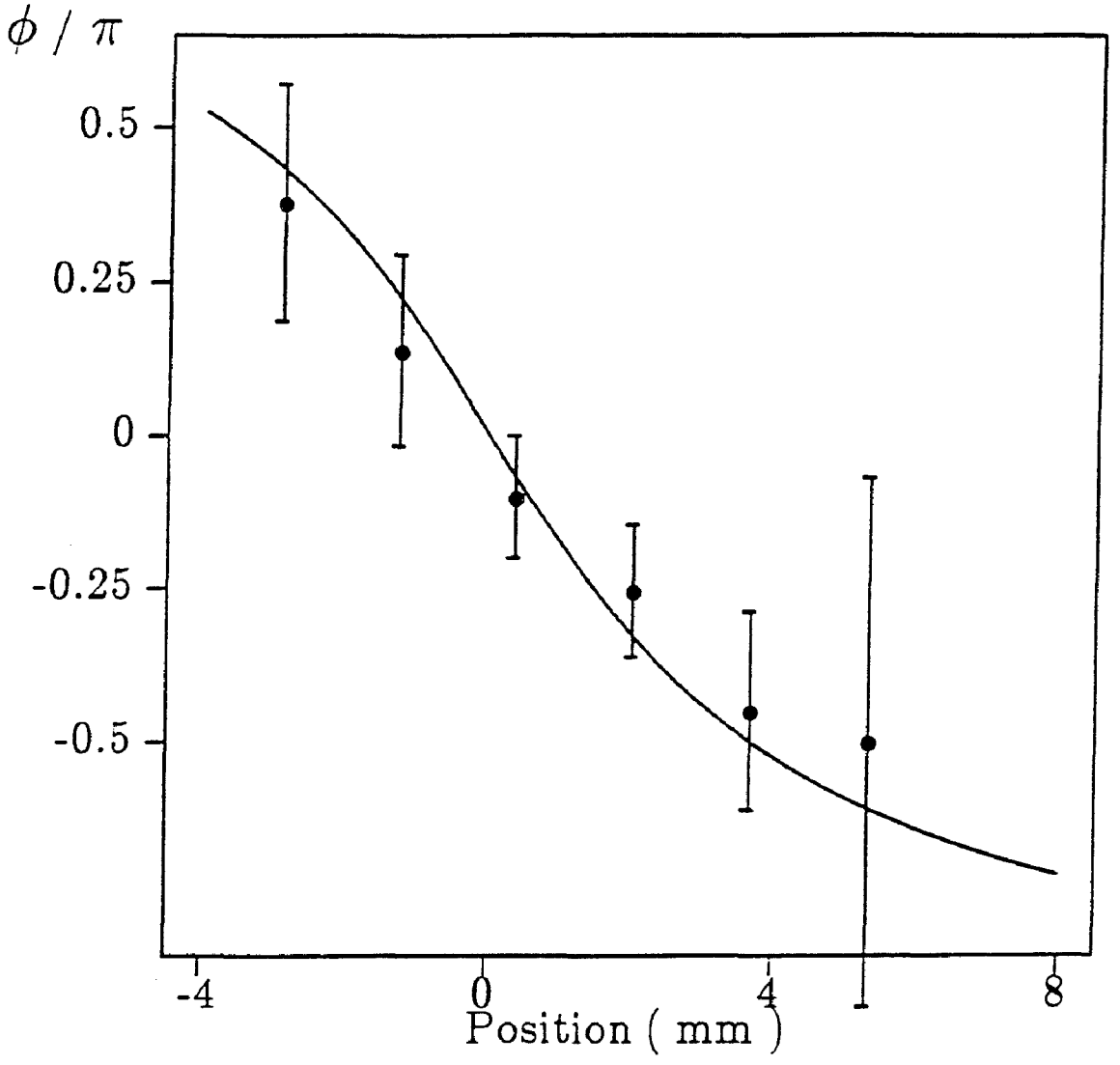

Figure 5.8. The relative phase of the ionization signal as a function of z, the distance from the laser beam focus, for $z_{0x} = 2.64$mm and $z_{0y} = 5.10$mm when a 17 cm lens is used.

laser beam of 554 nm was focused into the interaction cell. The signals collected by the electrodes are shown in Figure 5.9 as a function of the position of the electrodes. The solid line represents a z dependence of $\left\{[1+(\frac{z}{z_{0x}})^2][1+(\frac{z}{z_{0y}})^2]\right\}^{-1}$ fitted to the data by adjusting the amplitude and the position of the focus (z = 0 point). This z dependence corresponds to the intensity dependence of I^3, which means the ionization step after the atom has been excited to the 6p state is saturated. If we use a z dependence of $\left\{[1+(\frac{z}{z_{0x}})^2][1+(\frac{z}{z_{0y}})^2]\right\}^{-2}$, corresponding to a intensity dependence of I^5 and the case of nonsaturated ionization step, to fit to the data, the fitting error gets much bigger. This clearly indicates that the ionization step is saturated under the laser intensity used in the experiments. It seems that the efficiency of different electrodes varies and the spatial resolution of a set of only eight electrodes is not fine enough for a measurement of intensity dependence. Further improvements are needed.

So far the largest value for the depth of modulation we obtained for the ionization signal collected by the electrodes is about 58%. The limitations could be nonoptimal values of M, incomplete overlap of the two fields (transversely and longitudinally), imperfect $TEM_{0,0}$ laser beam and the "phase locking" related to local third-harmonic generation. The evidence showing that the "phase locking" is a main factor can be found in Table 5.1, in which we list values of the depth of modulation for different electrodes. The values are derived from data taken in three experiments under similar conditions. There is a clear tendency in these values that the depth of modulation for a certain electrode is lager than that for the next electrode, which is physically

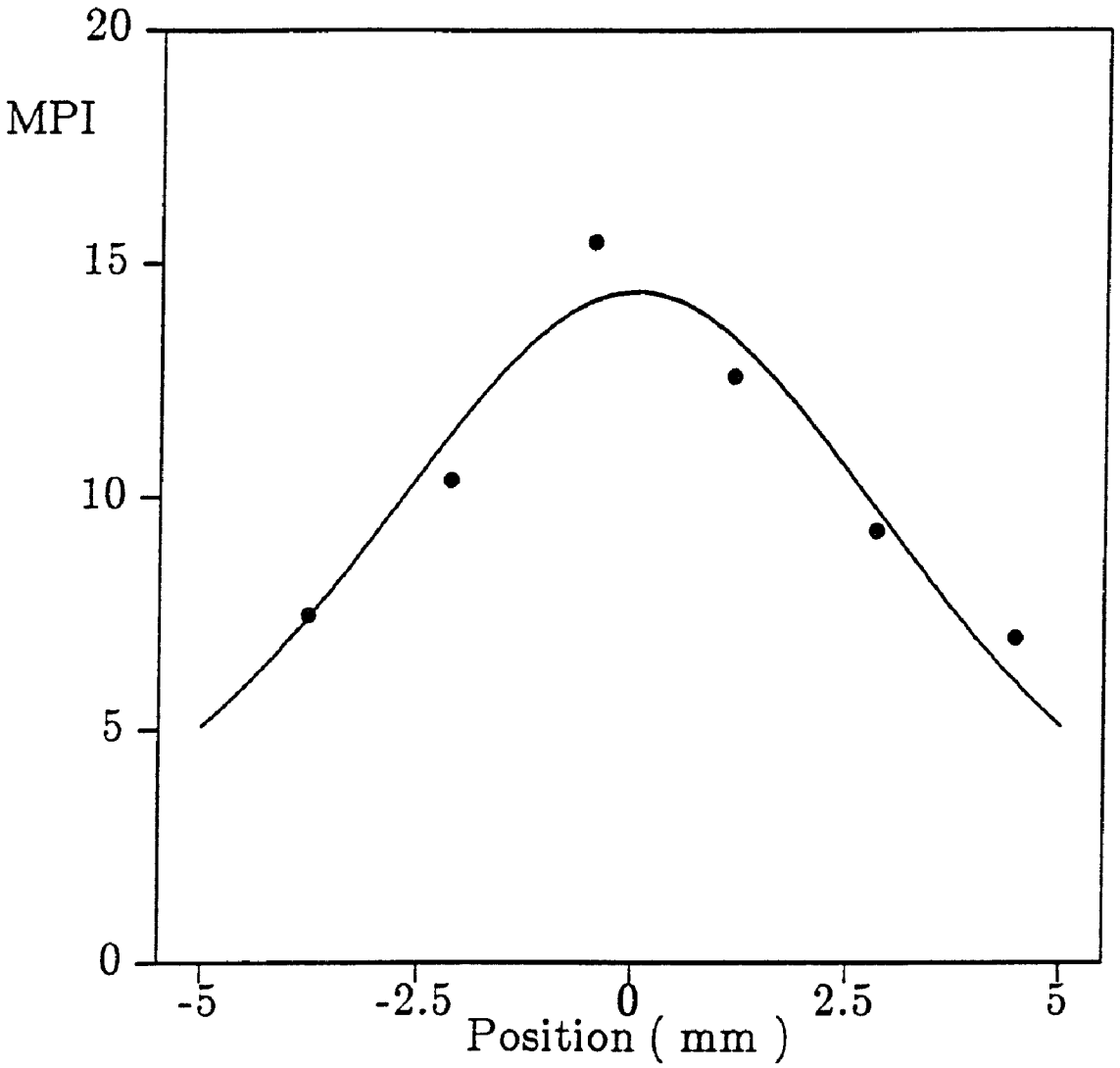

Figure 5.9. The ionization signal as a function of z, the distance from the laser beam focus. The generation cell was being cooled and evacuated when data was taken.

Electrode	1	2	3	4	5	6	7	8
Experiment 1	34%	29%	19%	17%	13%	12%	9%	/
Experiment 2	44%	45%	36%	36%	25%	17%	11%	/
Experiment 3	58%	33%	31%	28%	29%	29%	29%	/

Table 5.1. The depth of modulation of the ionization signal for different electrodes, derived from data taken in three experiments under similar conditions.

positioned behind it from the entrance port of the interaction cell. This tendency can hardly be explained by depletion of the third-harmonic field and strongly suggests the existence of the "phase locking" between the two fields.

Recently, we modified the experimental cells. First we replaced the two 25 cm focal length mirrors in the dispersion cell by two mirrors with 37.5 cm focal length and increased the path length of the fields inside the dispersion cell accordingly. This allows us to use higher intensity dye laser beam without burning the mirrors and improves the signal to noise ratio. Second we replaced the two parallel windows of 3/8 inch thickness by two 1/8 inch thick windows to reduce the window effects. The displacement between the focuses of the fundamental and the third-harmonic fields is about one third of

previously calculated 0.08 cm, resulting in a better longitudinal beam overlap. The modified cells provide a larger probability to get satisfactory results in interference experiments. The multi-photon ionization signal obtained by using the modified cells is shown in Figure 5.10. The experiment was carried out under similar conditions as that shown in Figure 5.6 except for a higher dye laser intensity of about 5.5 mJ/pulse. The smaller amount of argon pressure change required for a 2π phase change is due to the longer path length of the fields inside the dispersion cell.

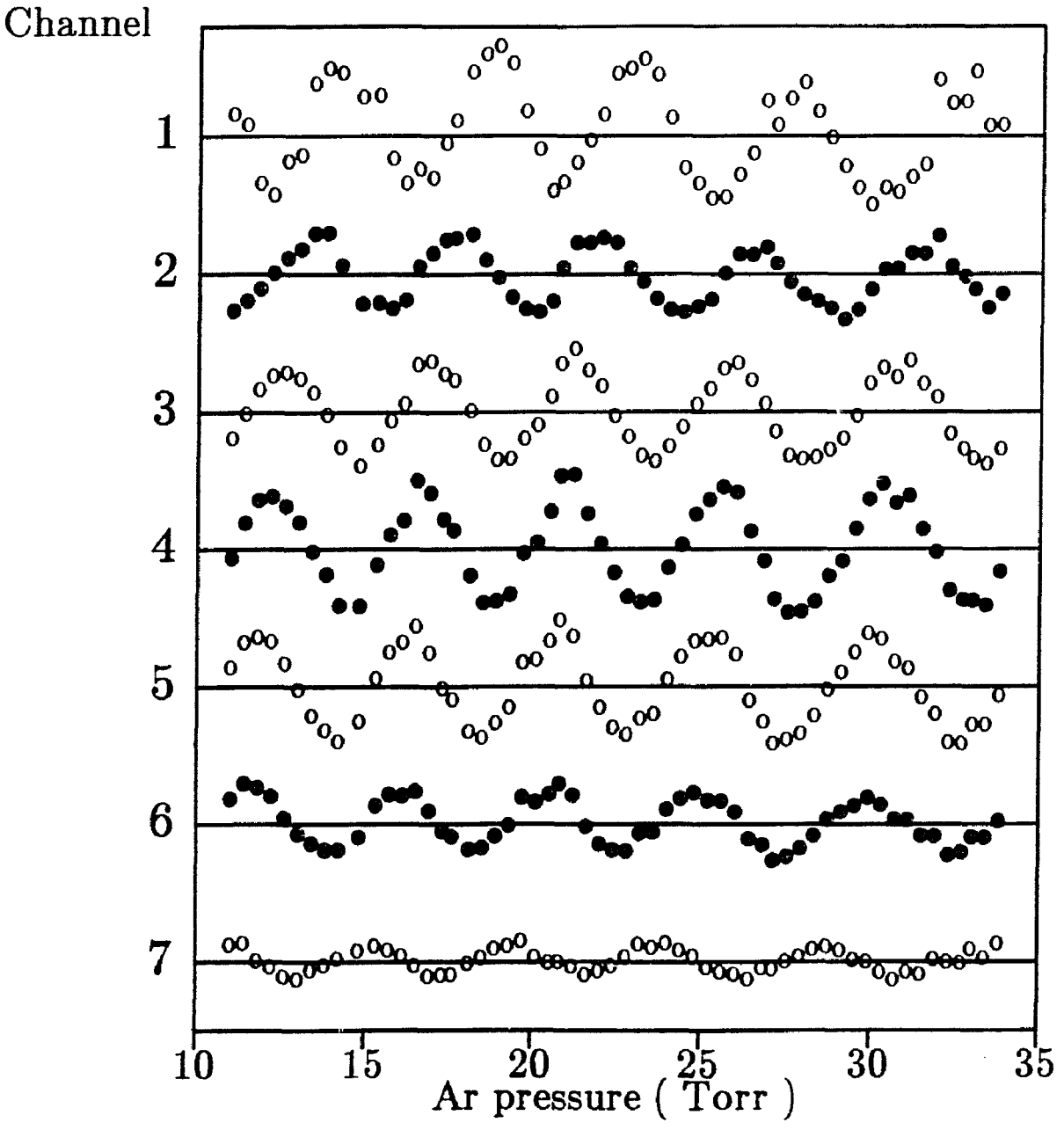

Figure 5.10. Ionization signal as a function of argon pressure for individual electrodes. The average DC level of the ionization signal has been subtracted from each data set. The experiment was carried out in the modified cells.

CHAPTER 6

CONCLUSIONS

In the interaction between an optical field and an atomic or molecular system, the phase of the field does not often produce direct observables. The observations of competing optical interactions [1-10] and this experimental study of interference between different optical processes are important exceptions to this rule. Because of the existence of two or more pathways induced by different fields, the interactions depend on the phase relations between the fields.

We experimentally studied the interference phenomena between one-photon and three-photon $6s^1S_0$ - $6p^1P_1$ transitions in a vapor of atomic mercury. Using a multi-cell design, we were able to separate the third-harmonic generation process and the interfering multi-photon ionization processes involving the one-photon and three-photon transitions. By changing the argon pressure in the dispersion cell, we were able to externally control the phase relation of the fundamental laser field and its third-harmonic and directly study the interference phenomena. We observed that the multiphoton ionization signal collected over the entire interaction region, which is a measure of the net transition moment from 6s to 6p states, varied sinusoidally with the change of the relative phase. The depth of modulation obtained in the total ionization signal was 15% out of a theoretically

maximum possible value of about 30%. Using an eight-electrode design to collect the electrons ionized at different distances from the focus along the beam axis, we measured the phase shift of the interference due to the π phase shift of a focused Gaussian beam propagating through its focal region. The data of phase shift obtained are in an excellent agreement with the calculated values. The multi-electrode structure has the potential to yield single-shot intensity dependence measurements. Our rough measurement of the intensity dependence indicates the existence of saturation in the multi-photon ionization under our experimental conditions. We also observed a decreasing tendency in the depth of modulation of ionization signal along the laser beam axis, which may provide an evidence to the "phase locking". We have constructed many experimental devices, set up the experimental apparatus and developed the experimental procedures. Similar experimental setup and methods can be applied to the studies of many phase sensitive processes including potential applications in coherent control of chemical reactions.

The experiments we have done are new and quite significant. However there is much room for improvements and future studies. For example, a more stable experimental system and a better control over the experimental conditions can produce quantitatively more repeatable measurements of the depth of modulation of the ionization signal. A lower noise and a more sensitive detection system will allow us to work at a lower mercury vapor density in the interaction region. A well calibrated multi-electrode detector, possibly with more than eight electrodes, will provide finer single-shot measurements of intensity dependence. All these improvements are needed in carrying out further investigation of this interference phenomenon.

The depth of modulation in the ionization signal is directly related to the value of M, which represents the ratio of the contributions of one-photon and three-photon transitions at the beam waist on focus. Studies of the relation between the depth of modulation and the mercury vapor density in the generation cell will lead to useful informations about the relative value of the three-photon and one-photon transition dipole moments. The depth of modulation in ionizations along laser beam axis is symmetric about the focus of the laser beams in the model we derived for ionization rate without consideration of phase locking which is due to local harmonic generation. Studies of the deviation of the depth of modulation from this symmetry at different mercury vapor density in the interaction cell will be a direct demonstration of the effect of the locally generated third-harmonic and provide a better understanding of the phase locking. There have been theoretical calculations [39] of phase locking in third-harmonic generation. A comparison between experimental observations and the theoretical calculations will be of a great interest.

Other experiments are being or will be carried out in our lab, such as interfering effect in photoelectron angular distribution, product-controlled photo-ionization of atoms and control of molecular photodissociation through two-path excitations. These experimental projects are closely related to the study of interfering multi-photon ionization in atomic mercury reported in this thesis. We are expecting exciting results from these experiments.

LIST OF REFERENCES

LIST OF REFERENCES

1. D. J. Jackson and J. J. Wynne, "Interference Effects between Different Optical Harmonics," *Phys. Rev. Lett.*, vol. 49, p. 543, 1982.

2. D. J. Jackson, J. J. Wynne and P. H. Kes, "Resonance-enhanced multiphoton ionization: Interference effects due to harmonic generation ," *Phys. Rev.*, vol. A 28, p. 781, 1983.

3. J. J. Wynne, "Polarization Renormalization Due to Nonlinear Generation ," *Phys. Rev. Lett.*, vol. 52, p. 751, 1984.

4. M. G. Payne and W. R. Garrett, "Theory of the effect of third-harmonic generation on three-photon resonantly enhanced multiphoton ionization in focused beams ," *Phys. Rev.*, vol. A 28, p. 3409, 1983.

5. J. C. Miller, R. N. Compton, M. G. Payne and W. R. Garrett, "Resonantly Enhanced Multiphoton Ionization and Third-Harmonic Generation in Xenon Gas," *Phys. Rev. Lett.*, vol. 45, p. 114, 1980.

6. J. C. Miller and R. N. Compton, "Third-harmonic generation and multiphoton ionization in rare gases," *Phys. Rev.*, vol. A 25, p. 2056, 1982.

7. J. H. Glownia and R. K. Sander, "Resonantly enhanced vacuum ultraviolet generation and multiphoton ionization in carbon monoxide gas ," *Appl. Phys. Lett.*, vol. 40, p. 648, 1982.

8. Y. I. Geller and A. V. Shvabauskas, "Influence of nonlinear frequency mixing on multiphoton ionization of gases ," *Opt. Spectrosc.*, vol. 53, p. 227, 1982.

9. S. A. Bakhramov, I. G. Kirin, P. K. Khabibullaev and N. S. Shaabdurakhmanova, "Influence of multiphoton ionization on frequency conversion in alkali metal vapors ," *Sov. J. Quantum Electron.*, vol. 12, p. 1557, 1982.

10. D. Normand. J. Morellec and J. Reif. "Resonant multiphoton ionization and third-harmonic generation in mercury vapour ," *J. Phys.*, vol. B 16, p. L 277, 1983.

11. M. S. Malcuit, D. J. Gauthier and R. W. Boyd, "Suppression of Amplified Spontaneous Emission by the Four-Wave Mixing Process ," *Phys. Rev. Lett.*, vol. 55, p. 1086, 1985.

12. A. V. Smith, *private communication.*

13. J. A. D. Stockdate, R. N. Compton, A. Dodhy, W. Christian, P. Lambropoulos and T. Olsen, "Laser-Induced Ionization and Stimulated Electronic Raman Scattering in Cesium Vapor ," *Multiphoton Processes, 4th International Conference*, p. 266, ed. by S. J. Smith, Boulder, 1987.

14. J. H. Glownia and R. K. Sander, "Experimental Evidence for the Competition between Resonantly Enhanced Multiphoton Ionization and Third-Harmonic Generation in Xenon," *Phys. Rev. Lett.*, vol. 49, p. 21, 1982.

15. S. Haroche, *High Resolution Spectroscopy, ed. K. Shimoda,* Springer-Veriag, Berlin, 1976.

16. M. Strand. J. Hansen, R. L. Chien and R. S. Berry, "Influence of Neclear Spin on Anglar Distribution and Polarization of Photoelectrons: Resonant Two-Photon Ionization of Na ," *Chem. Phys. Lett.*, vol. 59, p. 205, 1978.

17. G. Leuchs, S. J. Smith, E. Khawaja and H. Walther, "Quantum Beats Observed in Photoionization ," *Opt. Commun.*, vol. 31, p. 313, 1979.

18. J. E. Bjorkholm and P. F. Liao, "Reaonant Enhancement of Two-Photon Absorption in Sodium Vapor ," *Phys. Rev. Lett.*, vol. 33, p. 128, 1974.

19. J. Morellec, D. Normand, G. Mainfray and C. Manus, "First Experimental Evidence of Destructive Interference Effects in Two-Photon Ionization of Cs Atoms ," *Phys. Rev. Lett.*, vol. 44, p. 1394, 1980.

20. C. K. Chan, P. Brumer and M. Shapiro, "Coherent Radiative Control of IBr Photodissociation via Simultaneous (ω_1, ω_2) Excitation," *submitted to J. Chem. Phys.*.

21. P. Brumer and M. Shapiro, "Control of Unimolecular Reactions Using Coherent Light," *Chem. Phys. Lett.*, vol. 126, p. 541, 1986.

22. P. Brumer and M. Shapiro, "Coherent Radative Control of Unimolecular Reactions ," *Faraday Dis. Chem. Soc.*, vol. 82, p. 177, 1986.

23. M. Shapiro and P. Brumer . "Laser control of product quantum state populations in unimolecular reactions ," *J. Chem. Phys.*, vol. 84, p. 4103, 1986.

24. M. Shapiro, J. W. Hepburn and P. Brumer , "Simplified Laser Control of Unimolecular Reactions ," *Chem. Phys. Lett.*, vol. 149, p. 451, 1988.

25. C. Asaro, P. Brumer and M. Shapiro, "Polarization Control of Branching Ratios in Photodissociation ," *Phys. Rev. Lett.*, vol. 60, p. 1634, 1988.

26. P. Brumer and M. Shapiro, "Coherence Chemistry: Controlling Chemical Reactions with Lasers ," *Accounts Chem. Res.*, vol. 22, p. 407, 1989.

27. K. Aron and P. M. Johnson, "The Multiphoton Ionization Spectrum of Xenon: Interatomic Effects in Multiphoton Transitions," *J. Chem. Phys.*, vol. 67, p. 5099, 1977.

28. M. G. Payne, W. R. Garrett and H. C. Baker, "Effects of Collective Emission on Mulyiphoyon Excitation and Ionization Near a Three-photon Resonance," *Chem. Phys. Lett.*, vol. 75, p. 468, 1980.

29. M. G. Payne and W. R. Garrett, "Cooperative effects on multiphoton ionization and third harmonic generation in the region near three-photon resonance ," *Phys. Rev.*, vol. A 26, p. 356, 1982.

30. M. Poirier, "Competition between multiphoton ionization and third harmonic generation: A mean-field model ," *Phys. Rev.*, vol. A 27, p. 934, 1983.

31. R. N. Compton and J. C. Miller, "Two-color multiphoton ionization of xenon ," *J. Opt. Soc. Am.*, vol. B 2, p. 355, 1985.

32. S. P. Tewari and G. S. Agarwal, "Control of Phase Matching and Nonlinear Generation in Dense Media by Resonant Fields ," *Phys. Rev. Lett.*, vol. 56, p. 1811. 1986.

33. W. R. Garrett, S. D. Henderson and M. G. Payne, "Two-color Interference Effect Involving Three-photon Excitation and Four-wave Mixing Processes," *Phys. Rev.*, vol. A 34, p. 3463, 1986.

34. M. G. Payne, W. R. Garrett and W. R. Ferrell, "Three-photon resonantly enhanced multiphoton ionization and third-harmonic generation with unfocused laser beams ," *Phys. Rev.*, vol. A 34, p. 1143, 1986.

35. W. R. Garrett, W. R. Ferrell, M. G. Payne and J. C. Miller, "Influence of third-harmonic fields on multiphoton ionization of noble gases in unfocused laser beams ," *Phys. Rev.*, vol. A 34, p. 1165, 1986.

36. E. A. Manykin and A. M. Afanas'ev, "Resonance Phenomena in Nonlinear Optics," *Soviet Physics JETP*, vol. 21, p. 619, 1965.

37. G. L. Gurevich and Yu. G. Khronopulo, "Resonance Parametric Interaction of Strong Fields at Optical Frequencies," *Soviet Physics JETP*, vol. 24, p. 1012, 1967.

38. E. A. Manykin and A. M. Afanas'ev, "On One Possibility of Making a Medium Transparent by Multiquantum Resonance," *Soviet Physics JETP*, vol. 25. p. 828, 1967.

39. J. J. Wynne, "Nonlinear Optical Balance," *Multiphoton Processes: Proceedings of the 4th International Conference on Multiphoton Processes , ed. by S. J. Smith*, p. 318, Boulder,Colorado, 1987.

40. W. R. Garrett, "Influence of Internally Generated Fields on Odd Photon Pumping of Dipole-Allowed Transitions in Atomic Gases," *Multiphoton Processes: Proceedings of the 4th International Conference on Multiphoton Processes , ed. by S. J. Smith*, p. 328. Boulder,Colorado, 1987.

41. P. Brumer and M. Shapiro, "One Photon Mode Selective Control of Reactions by Rapid or Shaped Laser Pulses: An Emperor without Clothes?," *Chem. Phys.*, vol. 139, p. 221, 1989.

42. G. Kurizki, M. Shapiro and P. Brumer, "Phase-coherent control of photocurrent directionality in semiconductors ," *Phys. Rev.* , vol. B39, p. 3435, 1989.

43. T. Seideman, M. Shapiro and P. Brumer, "Coherent radiative control of unimolecular reactions: Selective bond breaking with picosecond pulses ," *J. Chem. Phys.*, vol. 90, p. 7132, 1989.

44. C. K. Chan, P. Brumer and M. Shapiro, "Interference between Optical Transitions and Control of Relative Cross Sections," *Phys. Rev. Lett. (Comments section)*, vol. 64, p. 3199, 1990.

45. J. F. Ward and G. H. C. New, "Optical Third Harmonic Generation in Gases by a Focused Laser Beam ," *Phys. Rev.*, vol. 185, p. 57, 1969.

46. C. Cuthbertson and M. Cuthbertson, *Proc. Roy. Soc.* , vol. 84, p. 13, London , 1910.

47. R. S. Finn and J. F. Ward, "Nonlinear-Optical Measurement of Dispersion in Gases ," *Appl. Optics*, vol. 11, p. 2103, 1972.

48. D. S. Elliott and J. F. Ward, "Measurements of refractive-index dispersion in gases with two-wavelength one-path interferometer ," *J. Opt. Soc. Am.*, vol. 73, p. 1836, 1983.

49. D. S. Elliott and J. F. Ward, "Polarizability Anisotropies of CO_2, N_2O, and OCS from Measurements of the Intensity-Dependent Refractive Index in Gases ," *Phys. Rev. Lett.*, vol. 46, p. 317, 1981.

50. J. Dudley and J. F. Ward, *Private communication.*

51. R. Loudon, *The Quantum Theory of Light,* pp. 73-75, Oxford University Press, Oxford, 1973.

52. A. Lurio, "Lifetime of the $6s6p\,^1P_1$ State of Mercury," *Phys. Review,* vol. 140, p. A1505, 1965.

53. M. G. Littman, "Single-mode pulsed tunable dye laser ," *Appl. Optics,* vol. 23, p. 4465, 1984.

54. C. Chen, Y. Yin and D. S. Elliott, "Interference between Optical Transitions," *Phys. Rev. Lett.*, vol. 64, p. 507, 1990.

55. A. Yariv, *Optical Electronics, 3rd Edition,* pp. 104-106, CBS College Publishing, New York, 1985.

56. C. Chen and D. S. Elliott, "Measurements of Optical Phase Variations Using Interfering Multiphoton Ionization Processes," *Phys. Rev. Lett.*, vol. 65, p. 1737, 1990.

VITA

VITA

Ce Chen was born in Shanghai, China in 1946. He received the BS degree in Physics from Fudan University, Shanghai in 1970, the MS degree in Physics from Fudan University in 1981.

He worked as a high school teacher for eight years and a university assistant professor for three years in China. Currently he is working towards his Ph.D. degree at the Electrical Engineering Department of Purdue University, West Lafayette, Indiana, U. S. A.